UNIVERSITÀ DEGLI STUDI DI CATANIA
Dipartimento di Ingegneria Elettrica Elettronica ed Informatica

Dottorato di Ricerca in Ingegneria Informatica e delle Telecomunicazioni
XXVI Ciclo

CIRCULARLY POLARIZED ANTENNAS

Ing. Ornella Leonardi

Coordinatore	Tutor
Chiar.ma Prof. V. Carchiolo	Chiar.mo Prof. G. Sorbello

Acknowledgment

I wish to thank my tutor Prof. Eng. Gino Sorbello for his unwavering support and encouragement over the last three years, for his generous mentorship and friendship. I consider it a privilege to have been his student. I have learned a tremendous amount from him, and his personal and professional example has meant a great deal to me.

I wish to thank Eng. Tindaro Cadili from Selex-ELSAG, site of Catania, for the use of the anechoic chamber facility to performed the experimental characterization of cross-slot coupled antenna.

I wish to thank Eng. Mario Pavone from StMicroelectronics for the experimental realization of elliptical-slot patch antenna.

I wish to thank Eng. Antonio Levanto from Technical Support Team ANSYS Electromagnetic for the countless loose knots in the use of HFSS simulator.

Also i wish to thank two great colleagues and friends, P. Di Mariano and L. Nicolosi, for their contribution to the experimental measurements and for their unwavering support and encouragement over the last year.

Most of all, I would like to thank my husband, Antonio, and my parents whose love, support and patience make this possible.

Contents

Abstract

In recent years low profile, lightness, compactness, easy manufacturing and integrability with solid-state devices on a circuit board have become a priority in the antenna design. Microstrip antennas are a possible answer to these new requirements in several areas, such as remote sensing, mobile satellite and cellular communications, direct broadcast satellite (DBS) system and global positioning system (GPS).

Many of the above mentioned applications make use of circularly polarized antennas. However, such requirement in planar microstrip antenna is not a trivial task since many factors have to be considered including fabrication tolerance and systematic errors in the manufacturing process.

In the present thesis we address the task to achieve circular polarization with very compact planar antennas in two ways:
1) a more conventional one dealing with two innovative designs;
2) a less conventional one through of artificial materials, such as High Impedance Surface (HIS).

As far as the first point is concerned, two standard designs have been developed for a Dedicated Short Range Communication (DSRC) system. In particular, we have proposed two innovative compact antennas that represent a step forward with respect to other available DSRC solution.

The two proposed antenna prototypes have been optimized, fabricated and experimentally tested. They represent an answer to the need of achieving good circularly polarized antennas in a small mobile On-Board Unit (OBU) of a DSRC system.

As a further study, we have considered to improve performance such as the radiated power, the gain and the directivity, or to reduce the global antenna thickness. For this reason we have developed a full-wave model for periodic surface and considered their employment to achieve circular polarization. As a proof of concept, we have tested a simple arrangement that allows circular polarization of the radiated field.

The thesis is organized as follows.

In the first part, we briefly introduce some relevant technical features of microstrip antenna's. Then the properties of circular polarized waves are discussed, with particular interest in wireless communications. The circular polarization quality factors and antenna measurement setup are briefly introduced and discussed.

In the second part, we address the design and the experimental characterization of two circularly polarized microstrip patch antenna prototypes.

In the last part of the thesis, High Impedance Surfaces (HIS) are briefly introduced. Then, a simple FEM-model is presented and compared with the standard FTDT-model used in literature. In this respect, a rectangular-array-patch working as HIS surface is considered and tested to achieve circular polarization with a printed dipole.

Chapter 1

Microstrip Antennas

In this chapter we discuss some of the microstrip antenna's technical features. We consider their advantages and disadvantages, including substrate material consideration, excitation techniques, polarization behaviors, bandwidth characteristics, and miniaturization techniques. The microstrip antenna radiation properties and analysis techniques are briefly presented.

1.1 Advantages and limitations

The microstrip antennas are nowday widely used in telecommunications systems, in fact they are employed in applications with working frequencies ranging from 100 MHz to 100 GHz, such as radar systems, satellite communications, mobile communications and wireless LAN. Their success is due to the many advantages of microstrip antennas compared to conventional counterparts. Among the advantage we list:

- relatively low production cost

- reduced volume and weight
- simpler integration with other electronic devices
- possibility to achieve linear and circular polarization with single feeding.

The major disadvantages of microstrip antennas are:

- higher ohmic and dielectric losses as compared to conventional solution
- low efficiency
- low directivity (6-8 dB)
- reduced gain (about 6 dB)
- high quality factor Q, which results in a very narrow bandwidth
- spurious radiation due to feed
- poor polarization purity
- complex electromagnetic analysis of the structure.

However, there are several methods to increase the radiation efficiency and the bandwidth, such as using structures with multiple substrate layers with different heights and dielectric constant. However complex multiple layer structure may support unwanted superficial waves that can be suppressed with the aid of special periodic structures known as AMC surface (see chapter 4).

Microstrip antennas consist of a very thin metallic *patch* ($17 < h_{metal} < 35\ \mu$m) separate from a ground plane by a dielectric *substrate*, with thickness $d << \lambda$ and with relative dielectric constants between in the range of $[2.2 \div 12]$. The metallic patches are the radiating elements and are usually photoetched on the dielectric substrate, these may be rectangular, circular, square, elliptical or any forms. The patch is connected to a RF source o to a receiver through a feeding line which can be a microstrip line. The main feeding techniques are discussed briefly in the next section.

Lower dielectric constant and thick substrate are desirable for antennas requiring high efficiency and larger bandwidth, whereas thin substrate and higher dielectric constants are required for feeding network where it is necessary to keep the fields well confined to avoid unwanted radiation and coupling losses. These requirements make it almost impossible to produce a good antenna on a single substrate. However, by separating the feed network from the radiating element, and providing aperture coupling between them it is possible to meet both the above requirements.

1.2 Feeding Methods

The feeding technique allow the control of the input impedance as well as the radiation characteristics of the antenna. The choice and optimization of feeding network is an important task in microstrip antenna design. The miscrostrip antenna can be excited directly either by a coaxial probe or by a microstrip line, otherwise indirectly using electromagnetic coupling through aperture coupling or by coplanar waveguide feed, in which case there is no direct metallic contact between the feed line and the patch.

The *coaxial or probe feed arrangement* requires that the center conductor of the coaxial connector is soldered to the patch. The main advantage of this feed is that the feeding point can be placed at any desired location inside the patch to match a desired impedance. The disadvantages are that the hole has to be drilled in the substrate and that the connectors protrudes outside the bottom ground plane, so that it isn't planar to the structure. Also this feeding arrangement makes the configuration asymmetrical.

The *microstrip line feed arrangement* (see figure 1.1 a) has the advantage that it can be etched on the same substrate, so the total structure remains planar. The drawback is the radiation from the feed line, which leads to an increase in the cross-polar level. Also, in the millimeter-wave range, the size of the feed line is comparable to the patch size, leading to increased undesired radiation.

In the *electromagnetic coupling feed arrangement* (see figure 1.1 b), also known as proximity coupling, a two dielectric layer structure is used and the feed line is placed between the patch and the ground plane. The advantages of this feed configuration include the reduction of spurious feed-network radiation. The disadvantages are that the two layers need to be aligned properly and that the overall thickness of the antenna increases.

In the *aperture-coupled arrangement* (see figure 1.1 c), the field is coupled from the microstrip line feed to the radiating patch through an electrically small aperture or slot cut in the ground plane. The coupling aperture is usually centered under the patch, leading to lower cross-polarization due to symmetry of the configuration. The slot aperture can be either resonant or not; in the first case provides another resonance in

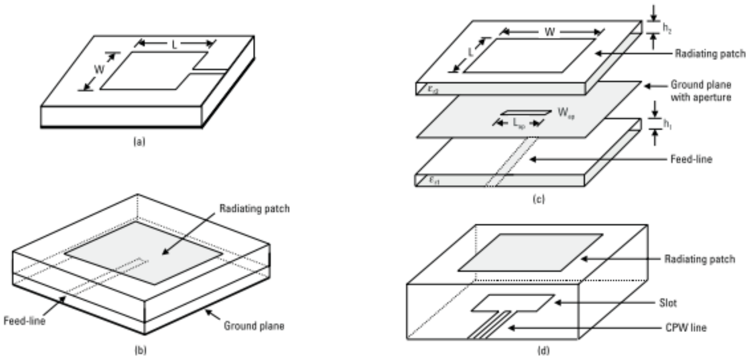

Figure 1.1: Feeding arrangements. (a) microstrip line, (b) electromagnetic coupling,(c) aperture coupling, and (d) coplanar waveguide (CPW).

addition to the patch resonance thereby increasing the bandwidth at the expense of an increase in back radiation.

In the *coplanar waveguide arrangement* (see figure 1.1 d) the CPW is etched on the ground plane of the microstrip. The coplanar waveguide is terminated by a slot. The main disadvantage of this method is the high radiation from the rather longer slot, leading to the poor front-to-back ratio. The front-to-back ratio can be improved by reducing the slot dimension and/or by modifying its shape, for example to form of a loop.

1.3 Antenna parameters and fundamental limitations

From the circuit point of view, an antenna is a single port device. An input signal in the form of an incident wave traveling along the transmission line flows from the signal source toward the antenna. Assuming the amplitude of the incident wave is V^+ at the antenna port, some of the energy carried by the incident wave is radiated by the antenna. In the meantime, the residual energy is reflected at the port and travels back along the transmission line. The amplitude of the reflected wave is V^-. The voltage reflection coefficient is given by:

$$\Gamma = \frac{V^-}{V^+}$$

When designing an antenna, the goal is to minimize the reflection at the antenna port, as low as possible ideally ($\Gamma \simeq 0$), that is make sure that a perfectly matched antenna is achieved.

In microwave theory, the S-parameter matrix is used to quantitatively describe a multi-port network. For an antenna its S-matrix degenerates to a single element, S_{11}, it is defined by the ratio of the voltages of incident and reflected wave, then:

$$S_{11} = \Gamma$$

In engineering the S_{11} is often defined as the ratio of incident and reflected power:

$$S_{11}(\mathrm{dB}) = 20\log_{10}(|S_{11}|)$$

The absolute value of S_{11} (dB) is called the Return Loss (RL):

$$RL = -S_{11}(\mathrm{dB})$$

The other commonly used parameter is Voltage Standing Wave Ratio (VSWR), it is the ratio of the amplitude of a partial standing wave at an antinode (maximum voltage) to the amplitude at an adjacent node (minimum voltage), in an electrical transmission line:

$$VSWR = \frac{|V_{max}|}{|V_{min}|}$$

Bandwidth is another important parameter used to describe antennas, it is defined as the frequency range over which a particular requirement is fulfilled. For example the impedance bandwidth is the frequency range over which VSWR is less than 2, which corresponds to a return loss of 9.5 dB or 11% reflected power. We defined the *fractional bandwidth* as the normalized spread between the half-power frequencies :

$$BW = \frac{f_{max} - f_{min}}{f_{operative}} = \frac{1}{Q}$$

where Q is the *Quality Factor*.
The quality factor is representative of the antenna losses:[1]

$$\frac{1}{Q} = \frac{1}{Q_{rad}} + \frac{1}{Q_c} + \frac{1}{Q_d} + \frac{1}{Q_{sw}}$$

where Q_{rad} is the contribution due to radiation losses, Q_c is the contribution due to conduction (ohmic) losses, Q_d is the contribution due to dielectric losses and Q_{sw} is the contribution due to surface waves.
For very thin substrate the losses due to surface waves are very small and can be neglected, while the Q_{rad} is inversely proportional to the height of the substrate and then it is usually the dominant factor.

The parameter which tells us how well an antenna can radiate is the *Efficiency*, it is the ratio of the power radiated by the antenna to the power delivered to the input terminals of the antenna, it is commonly expressed in dB :

$$\text{Efficiency (dB)} = 10 \log_{10} \frac{P_{radiated}}{P_{available}}$$

It can also be expressed in terms of the quality factors:

$$\text{Efficiency} = \frac{\frac{1}{Q_{rad}}}{\frac{1}{Q_c}}$$

---

[1] Balanis, *Antenna theory*, pag. 760-762.

The quality factor, bandwidth and efficiency are then antenna figures of merit which are correlated and there isn't complete freedom to independently optimize each one. Therefore there is always a trade-off between them to arriving at an optimum antenna performance.

1.4 Analysis Techniques: an overview

With an analysis technique, the engineer should be able to predict the antenna performance qualities, such as the input impedance, resonant frequency, bandwidth, radiation patterns, and efficiency. There are many different techniques of analysis for design microstrip antennas that can be divided into two broad categories:

- *analytical solution of an idealized model approximation*
- *numerical method*

In the first group make use of equivalence theorem and magnetic equivalent sources to model the patch edges, the most used are:

- *Transmission-line Circuit Model*[2]
- *Cavity Model*[3]
- *Multiport Network Model, MNM*[4]

---

[2] Munson, "Conformal microstrip antennas and microstrip phased arrays".

[3] Richards, Lo, and Harrison, "An improved theory for microstrip antennas and applications".

[4] Gupta and Sharma, "Segmentation and Desegmentation Techniques for the Analysis of Two Dimensional Microstrip Antennas".

Numerical method are based on the numerical solution of the distributions of real electric currents on the patch and the ground plane, between which the most important are:

- *Method of Moment, **MoM***[5]
- *Finite-Difference Time Domain, **FTDT***[6]
- *Finite-Element Method, **FEM***[7]

1.4.1 Approximate Models

In the *Transmission Line Model* the microstrip radiator element is viewed as a transmission line resonator with no transverse field variations, the field only varies along the length, and the radiation occurs mainly from the fringing fields at the open circuited ends. The patch is represented by two slots that are spaced by the length of the resonator. Although the Transmission Line Circuit Model is simpler than the cavity model, it gives good physical insight, but is less accurate and more difficult to model coupling.

The *Cavity Model* is more accurate but more complex. In the cavity model, the region between the patch and the ground plane is treated as a cavity that is surrounded by magnetic walls around the periphery and by electric walls from the top and bottom sides. Since thin substrates are used, the field inside the cavity is uniform along the thickness of the

---

[5] Newman and Tulyathan, “Analysis of microstrip antennas using moment methods”.

[6] Sheen et al., “Application of the three-dimensional finite-difference time-domain method to the analysis of planar microstrip circuits”.

[7] Silvester, “Finite element analysis of planar microwave networks”.

substrate. The fields underneath the patch for regular shapes can be expressed as a sum of the various resonant modes of a planar resonator. The effect of the fringing fields can be taken into account by extending the patch boundary outward, so that the effective dimensions are larger than the physical dimensions of the patch. The effect of the radiation from the antenna and the conductor loss are considered by adding these losses to the loss tangent of the dielectric substrate. The far field and radiated power are evaluated, using the equivalence theorem, from the equivalent magnetic current around the periphery (see 1.4.3).

The *Multiport Network Model* is an extension of the cavity model. In this method, the electromagnetic fields underneath the patch and outside the patch are modeled separately. The patch is analyzed as a two-dimensional planar network, with a multiple number of ports located around the periphery. The multiport impedance matrix of the patch is obtained from its two-dimensional Green's function. The fringing fields along the periphery and the radiated fields are incorporated by adding an equivalent edge admittance network. The segmentation method is then used to find the overall impedance matrix. The radiated fields are obtained from the voltage distribution around the periphery.

1.4.2 Numerical Models

The Numerical Methods, also known as *Full-Wave Model*, are very accurate, very versatile, but they are the most complex and the more expensive from a computational point of view.

In the MoM, the surface currents are used to model the microstrip patch, and volume polarization currents in the dielectric slab are used to model the fields in the dielectric slab. An integral equation is formulated for the unknown currents on the microstrip patches and the feed lines and their images in the ground plane. The integral equations are transformed into algebraic equations that can be easily solved using a computer. This method takes into account the fringing fields outside the physical boundary of the two-dimensional patch, thus providing a more exact solution.

The FEM, unlike the MoM, is suitable for volumetric configurations. In this method, the region of interest is divided into any number of finite surfaces or volume elements depending upon the planar or volumetric structures to be analyzed. These discretized units, generally referred to as finite elements, can be any well-defined geometrical shapes such as triangular elements for planar configurations and tetrahedral and prismatic elements for three-dimensional configurations, which are suitable even for curved geometry.

In the *FDTD Method* spatial as well as time grid for the electric and magnetic fields are generated. The solution is evaluated over such grids. The E cell edges are aligned with the boundary of the configuration and H-fields are assumed to be located at the center of each E cell. Each cell contains information about material characteristics. The cells containing the sources are excited with a suitable excitation, which propagates along the structure. The discretized time variations of the fields are determined at desired locations. Using a line integral of the electric field, the voltage across the two locations can be obtained. The current is computed by a loop integral of the magnetic field surrounding the conductor, where the Fourier transform yields a frequency response.

1.4.3 Cavity Model

Consider a simple microstrip patch antenna of any shape. Since the substrate has a thickness much smaller than both the wavelength and the size of the metal tracks, in first approximation, the electromagnetic field can be considered constant along the normal to the substrate. Initially we neglect the edge effect and we assume that the electric field has only a perpendicular component at the periphery of the substrate. This equals to ideally close transversely the perimeter of patch with Perfect Magnetic Conductor (PMC). In this way, the portion under the patch, for a rectangular patch, can be studied as a resonant cavity closed by four PMC walls and two PEC walls.

We assume that the EM field is independent of the $\widehat{z}$ coordinate orthogonal to the substrate, the electric field has only the component E_z while the magnetic field has transverse component, $\vec{H}_t$, with respect to $\widehat{z}$. By writing the solution of Maxwell's equations for TM fields as a function of a magnetic vectorial potential $\mathbf{A}(x, y) = A_z(x, y)\hat{z}$ and since $k_z = 0$, we have:

$$
\begin{aligned}
E_z(x,y) &= \frac{k^2}{j\omega\epsilon} A_z(x,y) = -j\omega\mu A_z(x,y) && (1.1)\\
\mathbf{H}_t(x,y) &= \nabla_t A_z(x,y) \times \hat{\mathbf{z}} = \frac{1}{j\omega\mu} \hat{\mathbf{z}} \times \nabla_t E_z(x,y) && (1.2)
\end{aligned}
$$

Then the electric field satisfy the two-dimensional Helmholtz's equation:

$$\nabla_t^2 E_z(x,y) + k^2 E_z(x,y) = 0 \tag{1.3}$$

with the boundary condition $\frac{\partial E_z}{\partial n} = 0$ where $\hat{n}$ is the unit vector orthogonal to the $\widehat{z}$ direction.

In Cartesian coordinates the equation (1.3) can be solved by the separation of variables method, then

$$\begin{aligned} E_z(x,y) &= X(x)Y(y) && (1.4)\\ X(x) &= C_1\sin(k_x x)+C_2\cos(k_x x) && (1.5)\\ Y(y) &= D_1\sin(k_y y)+D_2\cos(k_y y) && (1.6)\end{aligned}$$

where $k^2 = k_x^2 + k_y^2$.

Imposing the boundary condition $\frac{\partial E_z}{\partial n} = 0$ over the perimeter of patch and using the (1.2) we get:

$$\begin{aligned} E_z(x,y) &= C\cos\left(\frac{m\pi}{L}x\right)\sin\left(\frac{n\pi}{W}y\right) && (1.7)\\ H_x &= -\frac{1}{j\omega\mu}\frac{\partial E_z}{\partial y} = \frac{C}{j\omega\mu}\frac{n\pi}{W}\cos\left(\frac{m\pi}{L}x\right)\sin\left(\frac{n\pi}{W}y\right) && (1.8)\\ H_y &= \frac{1}{j\omega\mu}\frac{\partial E_z}{\partial x} = -\frac{C}{j\omega\mu}\frac{m\pi}{L}\sin\left(\frac{m\pi}{L}x\right)\cos\left(\frac{n\pi}{W}y\right) && (1.9)\\ k^2 &= \left(\frac{m\pi}{L}\right)^2+\left(\frac{n\pi}{W}\right)^2 \quad m,n=0,1,2... && (1.10)\end{aligned}$$

Because $k^2 = \omega^2\epsilon\mu$ the resonance frequency are achieved by:

$$f_{m,n} = \frac{c}{2\pi\sqrt{\epsilon_r}}\sqrt{\left(\frac{m\pi}{L}\right)^2+\left(\frac{n\pi}{W}\right)^2} \quad m,n=0,1,2... \qquad (1.11)$$

The cavity field for the fundamental mode TM$_{10}$ will be:

$$\begin{aligned} E_z(x) &= C\cos\left(\frac{\pi}{L}x\right) && (1.12)\\ H_y(x) &= -\frac{D}{j\omega\mu}\sin\left(\frac{\pi}{L}x\right) && (1.13)\end{aligned}$$

and the resonance frequency will be:

$$f_{1,0} = \frac{1}{2}\frac{c_0}{L\sqrt{\epsilon_r\mu_r}} \qquad (1.14)$$

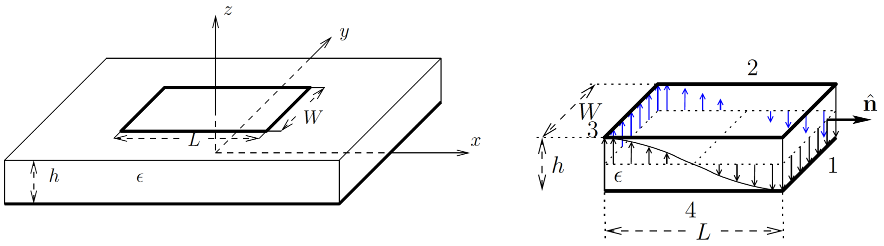

(a) (b)

Figure 1.2: Rectangular microstrip patch antenna: (a) new reference system; (b) Cavity Model. The Electric Field $\vec{E} = E_z(x)\widehat{u_z}$ is represented only around the perimeter at height $\frac{h}{2}$.

If we change reference frame equation (1.12)-(1.13) become:

$$\begin{cases} E_z(x) = -E_0 \sin\left(\frac{\pi}{L}x\right) \\ \\ H_y(x) = -H_0 \cos\left(\frac{\pi}{L}x\right) \end{cases} \tag{1.15}$$

To take account of the effects of the fringing fields we can consider an effective length in (1.14), where $L_{\text{eq}} = L + 2a$. The corrective term $2a$ is an empirical coefficient to account for the fringing of the electric field outside the patch.[8]

We proceed now to the calculation of the radiated field, making use of the Equivalence Theorem. Once the fields inside the cavity have been computed, the magnetic walls will be removed and you will evaluate the radiated field from the perimeter of the patch. Denote by R_1 the region

---

[8] Orfanidis, *Electromagnetic Waves and Antennas*, pag. 605.

within the cavity and with R_2 the surrounding space. As required by theorem we turn off all sources internal to the cavity and consider the equivalent currents on the lateral surface of this:

$$\left\{\begin{array}{l} \vec{J}_{m s \mathrm{eq}} = -\widehat{n} \times \vec{E}_2 \\ \\ \vec{J}_{s \mathrm{eq}} = \widehat{n} \times \vec{H}_2 \end{array}\right. \tag{1.16}$$

This system of equivalent currents flowing on the frontier of R_1 produces in R_2 an electromagnetic field identical to that generated by the real sources placed within R_1. We number the lateral faces of the cavity counterclockwise with increasing numbers.

As can be seen electrical currents are zero on faces 1, 2, 3 and 4, also magnetic current are zero on faces 1, 2, 3 and 4, since on faces 1 and 3 we have $H_y\left(\pm\frac{L}{2}\right) = 0$ and on faces 2 and 4 we have $\hat{n} \times \vec{H}_2 = \hat{u}_y \times H_y \hat{u}_y = 0$.

Magnetic current can be computed as follow:

$$\vec{J}_{m s \mathrm{eq}} = -\widehat{n} \times \vec{E}_2 \tag{1.17a}$$

where

$$\vec{E}_2(x) = -\vec{E}_0 \sin\left(\frac{\pi}{L} x\right) \tag{1.17b}$$

$$\begin{aligned} \vec{J}_{m s \mathrm{eq}_1} &= -\vec{E}_0 \widehat{u_y} && (1.18) \\ \vec{J}_{m s \mathrm{eq}_2} &= \vec{E}_0 \sin\left(\frac{\pi}{L} x\right) \widehat{u_x} && (1.19) \\ \vec{J}_{m s \mathrm{eq}_3} &= -\vec{E}_0 \widehat{u_y} && (1.20) \\ \vec{J}_{m s \mathrm{eq}_4} &= -\vec{E}_0 \sin\left(\frac{\pi}{L} x\right) \widehat{u_x} && (1.21) \end{aligned}$$

On face 1 and 3 the field is uniform because x is fixed: $x = \pm\frac{L}{2}$,

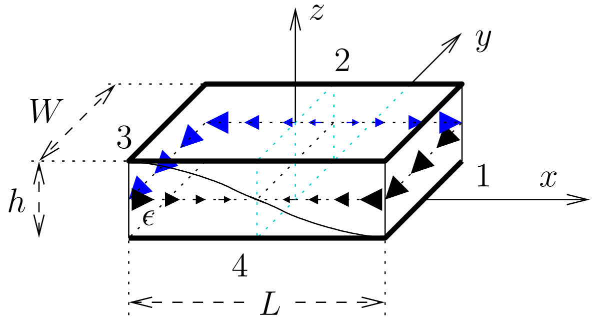

Figure 1.3: The equivalent magnetic current along the perimeter is represented only to the height $\frac{h}{2}$

while along the surface 2 and 4 the field varies with x, his dependence is obviously also for the equivalent magnetic currents (see figure 1.3).

On the faces 1 and 3, the electric field is uniform, but in the opposite direction, the normal outgoing from these sides are also in opposite directions, this means that the equivalent magnetic currents have the same direction. On faces 2 and 4 the electric field varies with the law $\sin\left(\frac{n}{L}x\right)$ and then have the same value in the form and sign, the normal outgoing from these sides are of the opposite direction, this means that the equivalent magnetic currents are opposite.

From the system of equivalent currents we can proceed to the calculation of the radiated fields. Since we are in presence of a ground plane we resort the theory of the image current. We remove the ground plane and consider equivalent currents (parallel to the ground plane) and current image with the same direction of the original currents, as shown in Figure 1.4.

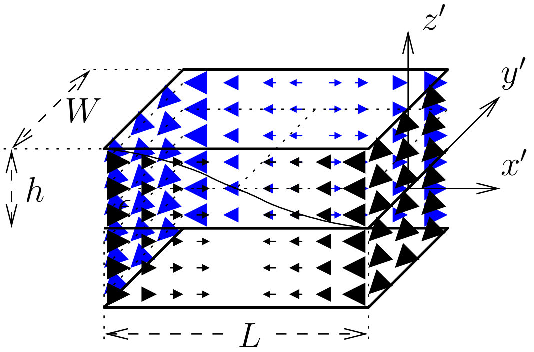

Figure 1.4: Magnetic currents resulting from the application of the Current Image Theorem

The radiated field is given by:

$$\vec{E}_{\mathrm{rad}} = -\frac{j}{2\lambda}\frac{e^{-\mathrm{jkr}}}{r}[L_\phi \widehat{u_\theta} - L_\theta \widehat{u_\phi}] \tag{1.22}$$

where L is given by:

$$\vec{L}(\theta,\phi) = \int_V \vec{J}_{0\mathrm{m}}(\vec{r'})\ e^{\mathrm{jk}\widehat{\mathrm{u_r}}\cdot\tilde{\mathrm{r}'}} dV' \tag{1.23}$$

We now proceed to calculate the radiation vector for each opening. The field due side 1 is:

$$\vec{E}_{\mathrm{rad1}} = \frac{j\vec{E}_0}{2\lambda}\frac{e^{-\mathrm{jkr}}}{r} 2Wh[\cos\phi\widehat{u_\theta} - \cos\theta\sin\phi\widehat{u_\phi}]\frac{\sin\left(\pi\frac{W}{\lambda}\sin\theta\sin\phi\right)}{\pi\frac{W}{\lambda}\sin\theta\sin\phi} \tag{1.24}$$

You can see from the above expression that the radiated field is proportional to the product Wh. In the design of power supply networks for microstrip antennas are often used stripline with width and substrate thickness h_{sub} reduced in order to avoid spurious radiation, viceversa for the patch is required thickness larger to increase the edge effects and increase the radiated field. This is the reason because the patch and the strip feed often are realized on two distinct planes, which are located at a different distance from the ground plane.

Slots 1 and 3 are called *radiant slots* and form an array of two elements, the array factor $A(\theta, \phi)$ is given by:

$$A(\theta, \phi) = 2\cos\left(\frac{\chi}{2}\right) \tag{1.25}$$

where $\chi = kd\cos\psi + \gamma$.

Because $d = L$ is the distance between the elements of the array, $\gamma = 0$ take into account any phase shifts of phase between the power of the elements of the array and $\cos\psi = \sin\theta\cos\phi$ takes account of the axis along which lie the elements of the array, we can write the array factor as follows:

$$A(\theta, \phi) = 2\cos\left(\frac{\pi L}{\lambda}\sin\theta\cos\phi\right) \tag{1.26}$$

The electric field radiated by the openings 1 and 3 is given by

$$\begin{gathered}\vec{E}_{\text{rad1,3}} = \frac{j\vec{E}_0}{2\lambda}\frac{e^{-\text{jkr}}}{r}4Wh\cos\left(\frac{\pi L}{\lambda}\sin\theta\cos\phi\right)\left[\,\cos\phi\widehat{u_\theta}\;-\cos\theta\sin\phi\widehat{u_\phi}\,\right]\cdot \\ \cdot\frac{\sin\left(\pi\frac{W}{\lambda}\right)\sin\theta\sin\phi}{\pi\frac{W}{\lambda}\sin\theta\sin\phi}\end{gathered} \tag{1.27}$$

The total field radiated by the antenna is made up mainly from the effects of radiation due to slots 1 and 3 as the sides 2 and 4 present current opposite to each other. The current on side 2 is sinusoidal, then the effects tend to cancel already on the single side, if we observe simultaneously slots 2 and 4 currents are opposite two by two, so if the two sides were coincident these contributions will cancel. In reality $\vec{E}_{rad2,4}$ is not identically zero because the current does not cancel out perfectly, but do not make a great mistake if the computation of the radiated field slots 2 and 4 are neglected. The expression 1.26 the array factor has the maximum in the plane transverse to the alignment direction of the currents, the plane yz, characterized by $\phi = \frac{\pi}{2}$. The expression 1.26 the array factor has the maximum in the plane transverse to the alignment direction of the currents, the plane yz, characterized by $\phi = \frac{\pi}{2}$. The electric field of the single element of the array ($\vec{E}_{rad1}$) presents the maximum for $\phi = 0$, ie in the plane xz, then the direction of maximum radiation of the product is z axis, because in this direction maximize both factors. The polarization of the radiated field is that of the single element and is directed along resonant length L.

Chapter 2

Circular Polarization

The polarization of the electric field $\vec{E}$ is an important property of the electromagnetic wave propagation radiated by an antenna.

The polarization is defined by the shape and orientation of the locus of the extremity of the electric field vectors as a function of time. Suppose we have two antennas placed one in a farfield other. Denote by $\hat{\mathbf{k}}_{\mathrm{tx}}$ the unit propagation vectors of the wave radiated by the transmitting antenna and by $\hat{\mathbf{k}}_{\mathrm{rx}}$ the unit propagation vectors of the wave radiated by the receiving antenna, if it placed in transmission. P_r is the total power radiated from the transmitted antenna and P_d the power available at the output section of the receiving antenna, both in input-impedance matching. The power P_d depends by the incident power density $S_{inc} = \frac{|\vec{\mathbf{E}}_{\mathrm{inc}}|^2}{2\eta}$, by the polarization of the incident wave radiated from the transmitting antenna $\vec{\check{\mathbf{p}}}_{\mathrm{inc}} = \frac{\vec{\mathbf{E}}_{\mathrm{inc}}}{|\vec{\mathbf{E}}_{\mathrm{inc}}|}$, by source direction of the incident wave $\hat{\mathbf{k}}_{\mathrm{tx}}$, namely by relative orientation between the receiving antenna and the incident wave:

$$P_d = A(\vec{\check{\mathbf{p}}}_{\mathrm{inc}}, \hat{\mathbf{k}}_{\mathrm{tx}}) S_{inc} \qquad (2.1)$$

where $A(\vec{\check{\mathbf{p}}}_{\text{inc}}, \hat{\mathbf{k}}_{\text{tx}})$ is a proportionality constant known as the *effective area.*

The effective area of the incident wave can be write as:

$$A(\vec{\check{\mathbf{p}}}_{\text{inc}}, \hat{\mathbf{k}}_{\text{tx}}) = \frac{\lambda^2}{4\pi} G_t(\hat{\mathbf{k}}_{\text{rx}}) \left| \vec{\check{\mathbf{p}}}_{\text{inc}} \cdot \vec{\check{\mathbf{p}}}(\hat{\mathbf{k}}_{\text{rx}}) \right|^2 \tag{2.2}$$

where $G_t(\hat{\mathbf{k}}_{\text{rx}})$ is the receiving antenna gain when it is places in transmission.

The term

$$\tau = \left| \vec{\check{\mathbf{p}}}_{\text{inc}} \cdot \vec{\check{\mathbf{p}}}(\hat{\mathbf{k}}_{\text{rx}}) \right|^2 \tag{2.3}$$

is said *polarization mismatch factor.*

The polarization mismatch factor is defined as the ratio of the power actually received by the antenna divided by the power that would be received from a polarization matched incoming wave. It has value between 0 and 1, if $\tau = 1$ the received power is maximized, while if $\tau = 0$ no power is detect.

Substituting (2.2) into (2.1) and remembering that the incident power density is equal to $S_{inc} = \frac{P_r}{4\pi r^2}\, G_t(\hat{\mathbf{k}}_{\text{tx}})$ where $G_t(\hat{\mathbf{k}}_{\text{tx}})$ is the gain of transmitted antenna, is obtained

$$P_d \;=\; P_r \left(\frac{\lambda}{4\pi r} \right)^2 \, G_t(\hat{\mathbf{k}}_{\text{rx}}) \; G_t(\hat{\mathbf{k}}_{\text{tx}}) \; \tau \tag{2.4}$$

where $\left(\frac{\lambda}{4\pi r}\right)$ is called *free-space loss factor*, it takes into account the power density reduction due to the spherical spreading of the energy radiated by the antenna. For polarization matched antennas oriented in such a way that one is in the direction of maximum gain of the other, and viceversa, the power P_d is maximum and equal to:

$$P_d \;=\; P_r G_1 G_2 \left(\frac{\lambda}{4\pi r} \right)^2 \tag{2.5}$$

where $\tau = 1$ and G_1 and G_2 are the maximum gains.

The use of linear polarized signals can lead to the loss of connection if the transmitting and receiving antennas are orthogonally oriented, the received signal would ideally be zero. This problem can be overcome by using circularly polarized antennas since the polarization factor is independent from the mutual orientation of the two antennas.

A perfectly circularly polarized wave is generated by an antenna that simultaneously excites two linearly polarized wave of equal amplitude and in phase quadrature. Formal definitions for this mode of propagation are given in the IEEE Standard Test Procedures for Antennas[1] , where the sense of polarization is defined as the sense of rotation of the extremity of the electric field for an observer looking in the propagation direction.

Consider the superposition of an $\widehat{x}$ linearly polarized wave with amplitude E_x and a $\widehat{y}$ linearly polarized wave with amplitude E_y, both traveling in the positive $\widehat{z}$ direction. The total electric field can be written as:

$$\vec{E}(z,t) = (E_x\widehat{x} + E_y\widehat{y})e^{-jk_0 z}e^{j\omega t} \tag{2.6}$$

Precisely polarization is the direction of the time-varying real-valued field $\mathbf{E}(z,t) = Re[\vec{E}(z,t)]$, at any fixed point z. The corresponding real-valued x and y components are:

$$E_x(z,t) = A\cos(\omega t + kz + \phi_a) \tag{2.7}$$

$$E_y(z,t) = B\cos(\omega t - kz + \phi_b) \tag{2.8}$$

To determine the polarization of the wave, we consider the time-dependence of these fields at some fixed point along the z-axis, say at

---

[1] Standard, "IEEE Standard Test Procedures for Antennas", section 11, pag. 61.

z=0:

$$E_x(t) = A\cos(\omega t + \phi_a) \tag{2.9}$$

$$E_y(t) = B\cos(\omega t + \phi_b) \tag{2.10}$$

The electric field vector $\vec{E}(t) = E_x(t)\widehat{x} + E_y(t)\widehat{y}$ will be rotating on the xy-plane with angular frequency ω, with its tip tracing, in general, an ellipse. To see this, we expand (2.9) and (2.10) using a trigonometric identity:

$$E_x(t) = A[\cos\omega t\cos\phi_a - \sin\omega t\sin\phi_a] \tag{2.11}$$

$$E_y(t) = B[\cos\omega t\cos\phi_b - \sin\omega t\sin\phi_b] \tag{2.12}$$

Solving for $\cos\omega t$ and $\sin\omega t$ in terms of $E_x(t)$ and $E_y(t)$ we find:

$$\cos\omega t\cos\phi = \frac{E_y(t)}{B}\sin\phi_a - \frac{E_x(t)}{A}\sin\phi_b \tag{2.13}$$

$$\sin\omega t\sin\phi = \frac{E_y(t)}{B}\cos\phi_a - \frac{E_x(t)}{A}\cos\phi_b \tag{2.14}$$

where we defined the relative phase angle $\phi = \phi_a - \phi_b$.

Forming the sum of the squares of the two equations and using the trigonometric identity $\sin^2\omega t + \cos^2\omega t = 1$ we obtain a quadratic equation for the components E_x and E_y, which describes an ellipse on the E_x and E_y plane:

$$\left(\frac{E_y(t)}{B}\sin\phi_a - \frac{E_x(t)}{A}\sin\phi_b\right)^2 + \left(\frac{E_y(t)}{B}\cos\phi_a - \frac{E_x(t)}{A}\cos\phi_b\right)^2 = \sin^2\phi \tag{2.15}$$

This simplifies into:

$$\frac{E_x^2}{A^2} + \frac{E_y^2}{B^2} - 2\cos\phi\frac{E_xE_y}{AB} = \sin^2\phi \tag{2.16}$$

To get circular polarization, we set $A = B$ and $\phi = \pm\pi/2$, in this case, the polarization ellipse becomes the equation of a circle:

$$\frac{E_x^2}{A^2} + \frac{E_y^2}{B^2} = 1 \tag{2.17}$$

2.1 Axial Ratio and XPD

The sense of a circularly polarized wave is determined by the rotation direction of the vector $\vec{E}$ as it describes a circle; a right-hand circular polarization (RHCP) signal is generated when the rotation direction is clockwise, while for a left-hand circular polarization (LHCP) wave the vector rotates counterclockwise when the observer is placed in the direction of propagation.

For the case $\phi_a = 0$ and $\phi_b = -\pi/2$ we have $\phi = \phi_a - \phi_b = \pi/2$ and

$$E_x(t) = A\cos\omega t \tag{2.18}$$

$$E_y(t) = B\cos(\omega t - \pi/2) = A\sin\omega t \tag{2.19}$$

thus the tip of the electric field vector rotates counterclockwise on the xy-plane then the polarization is left polarized.

Instead for the case $\phi = -\pi/2$, arising from $\phi_a = 0$ and $\phi_b = \pi/2$, we have

$$E_x(t) = A\cos\omega t \tag{2.20}$$

$$E_y(t) = B\cos(\omega t + \pi/2) = -A\sin\omega t \tag{2.21}$$

thus the tip of the electric field vector rotates clockwise on the xy-plane then the polarization is right polarized.

A practical antenna usually generates an imperfect circularly polarized field, therefore the vector traces out an ellipse instead of a circle.

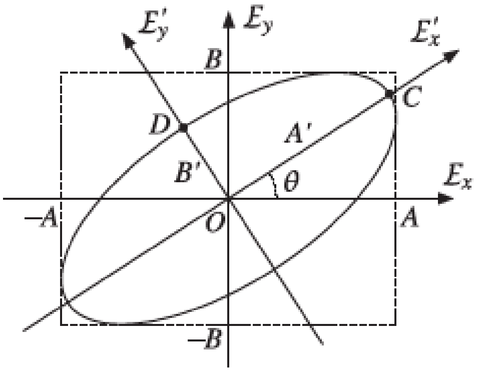

Figure 2.1: Polarization Ellipse

The spatial orientation of the major to minor axes defines the *tilt angle*, ψ, in the clockwise direction between a reference position and the major axis looking in the direction of propagation:

$$\tan 2\psi \quad = \quad \frac{2AB}{A^2 - B^2} A \cos\phi \tag{2.22}$$

To provide maximum coupling in point-to-point communication systems the two antennas must be polarization-matched and their tilt angles have to be aligned.

The ratio of the major to minor axes defines the *Axial Ratio* (AR) of the polarized wave; for perfect CP wave propagation, where only one hand of polarization is generated, the AR will have a value of 1. In the extreme case where the magnitude of the RHCP and LHCP components are the same, the circle formed by the tip of the vector degenerates into a line, the polarization becomes linear, and the AR value becomes infinite. In practical applications, a field is considered circularly polarized when AR is less than 3 dB, however in many applications an AR of 6 dB is acceptable.

A real antenna normally generates a desired reference polarization in addition to an undesirable cross-polar component, which is polarized in the opposite hand. In the main beam, the ratio between the power level of the reference wave and the undesirable component is defined such as *Cross-Polar Discriminator* (XPD) at a given azimuth angle. For a perfectly circularly polarized pattern, this level is $-\infty$ dB, and for a linearly polarized field, where the two CP signals are of identical magnitude, this level is 0 dB. XPD quantifies the separation between two transmission channels that use different polarization orientations.

The AR is related to cross-polarization by following formula[2] :

$$XPD = \left[\frac{AR+1}{AR-1}\right]^2 \tag{2.23}$$

2.2 Methods to achieve Circular Polarization

For a patch antenna, circular polarization can be obtained if two orthogonal modes are excited with a 90° time-phase difference between them. This can be achived by modifying the geometry of the patch, by inserting slots, slit or tabs, or by using two o more feeds.

For a rectangular patch the easiest way to achieved circularly polarization is to feed the patch at two adjacent edge and for circular patch to feed at two proper angular separation[3] , the quadrature phase is

---

[2] Toh, Cahill, and Fusco, “Understanding and measuring circular polarization”.

[3] Richards, Lo, and Harrison, “An improved theory for microstrip antennas and applications”.

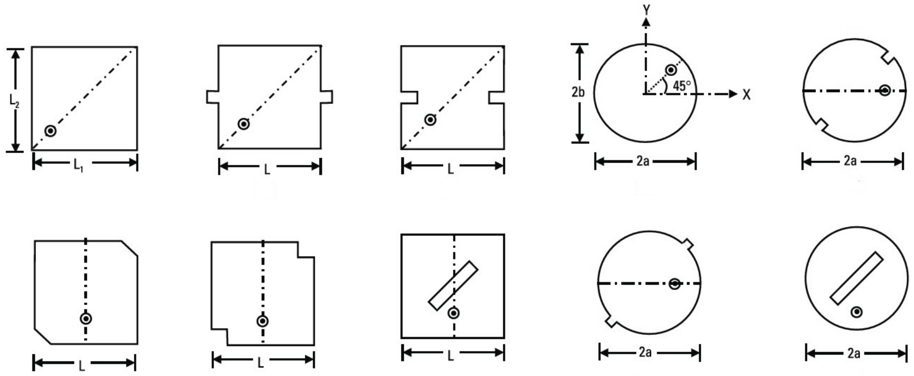

Figure 2.2: Single-feed configuration to obtain CP

obtained by feeding the two feeds with a 90-degree power divider or hybrid.[4]

To overcome the complexities of dual-feed arrangements, CP can also be achieved with a single feed, in this configurations the principle to obtain the CP is same. The antenna is a diagonally fed nearly square patch, or square patch with stubs and notches along the two opposite edges, or corner-chopped squares, or squares with a diagonal slot. Many others configuration are possible (see figure 2.2).

The dimensions of the patch are modified such that the resonance frequencies f_1 and f_2 of the two orthogonal modes are close to each other. The antenna is excited at a frequency f_0 in between the resonance frequencies of these two modes, such that the magnitude of the two excited modes are equal. Also, the feed-point location is selected in such a way that it excites the two orthogonal modes with phase difference of $+45°$

---

[4] Balanis, *Antenna theory*.

and −45° with respect to the feed point, which results in phase quadrature between the two modes.[5][6] These two conditions are sufficient to yield CP. A similar result is obtained by modifying at the same way a circular or triangular patch configurations with a single feed[7][8][9][10] .

A further technique to obtain circular polarization consists in exciting the patch by a linear aperture[11][12] or by modifying the aperture itself[13] located on the ground plane. These techniques, often used in multilayered structures, have the beneficial effect of increasing the bandwidth.

Circular polarization can be obtained also using the sequentially rotated array configuration, the single elements could be linearly[14] or circularly polarized. In the first case the technique provides that an array of 2 or 4 patch positioned orthogonally to each other are fed by equal magnitude through a power divider and with a 90° mutual phase difference. The performance of the circularly polarized antenna array can be

---

[5] Richards and Lo, “Design and theory of circularly polarized microstrip antennas”.

[6] Lo, Engst, and Lee, “Technical memorandum: Simple design formulas for circularly polarised microstrip antennas”.

[7] Iwasaki, “A circularly polarized small-size microstrip antenna with a cross slot”.

[8] Wong and Lin, “Circularly polarised microstrip antenna with a tuning stub”.

[9] Hsieh, Chen, and Wong, “Single-feed dual-band circularly polarised microstrip antenna”.

[10] Lu, Tang, and Wong, “Circular polarisation design of a single-feed equilateral-triangular microstrip antenna”.

[11] Aksun, Chuang, and Lo, “On slot-coupled microstrip antennas and their applications to CP operation-theory and experiment”.

[12] Huang, Wu, and Wong, “Cross-slot-coupled microstrip antenna and dielectric resonator antenna for circular polarization”.

[13] Pozar, “A reciprocity method of analysis for printed slot and slot-coupled microstrip antennas”.

[14] Huang, “A technique for an array to generate circular polarization with linearly polarized elements”.

increased by using N linearly polarized elements arranged in a circular ring geometry, this N elements are placed at an angle of $360/N$ degrees with respect to each other and are sequentially fed to generate CP response. The feed phase of each individual element is arranged in steps of $\phi_n = 2\pi(n-1)/N$ where $n = 1, 2, ...N$.[15] Using circular polarized patches the technique of sequential rotation allows to improve the purity of polarization and bandwidth[16] .

2.3 Antenna Measurement

It is usually convenient to perform antenna measurements with the test antenna in its receiving mode because it is assumed that the test antenna can be treated as a passive, linear, and reciprocal device. The ideal condition for measuring farfield radiation characteristics is the illumination of test antenna by plane waves: with uniform amplitude and phase. This condition can be approximated by separating the test antenna from the illumination source by a large distance equal to the inner boundary of the farfield region, $r > (2D^2/\lambda)$[17] . At this distance the curvature of the spherical phasefront produced by the source antenna is small over the test antenna aperture but reflections from the ground and nearby object are possible sources of degradation of the test antenna.

A spherical coordinate system can be associated with the antenna under test, see figure 2.3. The antennas coordinate system is typically

---

[15] Teshirogi, Tanaka, and Chujo, “Wideband circularly polarized array antenna with sequential rotations and phase shift of elements”.

[16] Jazi and Azarmanesh, “Design and implementation of circularly polarised microstrip antenna array using a new serial feed sequentially rotated technique”.

[17] Cutler, King, and Kock, “Microwave antenna measurements”.

defined with respect to a mechanical reference on the antenna.

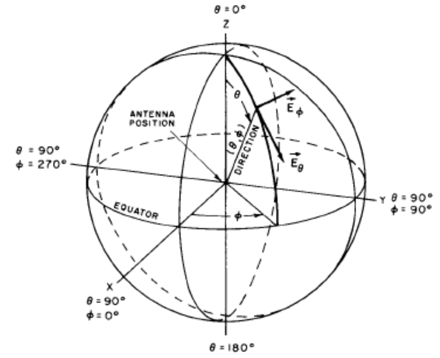

Figure 2.3: Standard spherical coordinate system used in antenna measurements

There are situations in which the operational antenna illuminates structures in its immediate vicinity; this can modify the radiation field of the isolated antenna. In these cases it may be necessary for measurements of the radiation field to include with the antenna those relevant parts of the nearby structures. The use of scale models is quite common for such cases[18] .

To completely characterize the radiation field of an antenna, one shall measure its relative amplitude, relative phase, polarization, and the power gain on the surface of a sphere centered where the antenna under test is located. A representation of any of these radiation properties as a function of space coordinates is defined as a *radiation pattern.*

Since the distance r from the antenna under test to the measuring point is fixed, only the two angular coordinates are variables in a given

---

[18] Standard, "IEEE Standard Test Procedures for Antennas", section 7.1.

radiation pattern. Usually the operation frequency is treated as a parameter, with the radiation pattern being measured at specified frequencies. If frequency is varied continuously, such a procedure is called a *swept-frequency technique.*[19]

A direct method of measuring the radiation pattern of a test antenna is to employ a suitable source antenna, which can be positioned in such a manner that it moves relative to the test antenna along lines of constant θ and constant ϕ: measurements made with ϕ as the variable and θ as a fixed parameter are called conical cuts or ϕ cuts, while those made with θ as the variable and ϕ as a parameter are called great-circle cuts or θ cuts. Note that the cut for $\theta = 90^\circ$ is also a great-circle cut. Principal-plane cuts refer to orthogonal great-circle cuts which are through the axis of the test antennas major lobe. For this definition to hold, the beam axis shall lie either in the equator of the spherical coordinate system ($\theta = 90^\circ$) or at one of the poles ($\theta = 0^\circ$ or $\theta = 180^\circ$). Principal plane cuts for linear polarization are usually defined, these would be in the E plane and the H plane of the test antenna.

There are two basic range configurations that accomplish the position requirement for θ and ϕ cuts. One is the *fixed-line-of-sight configuration*, here the test antenna and its associated coordinate system are rotated about an axis passing through the phase center of the test antenna. If the test antenna is operating in the receive mode, then the signal that it receives from an appropriately located fixed source antenna is recorded. The other one is called the *movable-line-of-sight configuration*, for this case the source antenna is moved incrementally or continuously along the circumference of a circle centered approximately at the phase center of the

---

[19] Standard, "IEEE Standard Test Procedures for Antennas", chapter 7.4.

antenna under test. If it is moved incrementally, then for each position of the source antenna the test antenna is rotated and the received signal is recorded. Alternatively the test antenna can be rotated incrementally, and for each of its positions the source antenna is moved continuously along its circumferential path.

If the test antenna and the source antenna are both reciprocal devices, the functions of receive and transmit may be interchanged. The measured transmitted and received patterns should be identical. In the following, unless otherwise stated, the test antenna shall be considered as the receiving antenna, and it will be illuminated by the field of the transmitting source antenna.

In the case of the fixed-line-of-sight system the θ and ϕ rotations are provided completely by the positioner for the test antenna. Two positioners which meet the requirements for this system are the azimuth-over-elevation and the elevation-over-azimuth types. These positioners and their associated coordinate systems are shown in figure 2.4.
An example of an elevation-over-azimuth positioner is the Model Tower (see figure 2.5).

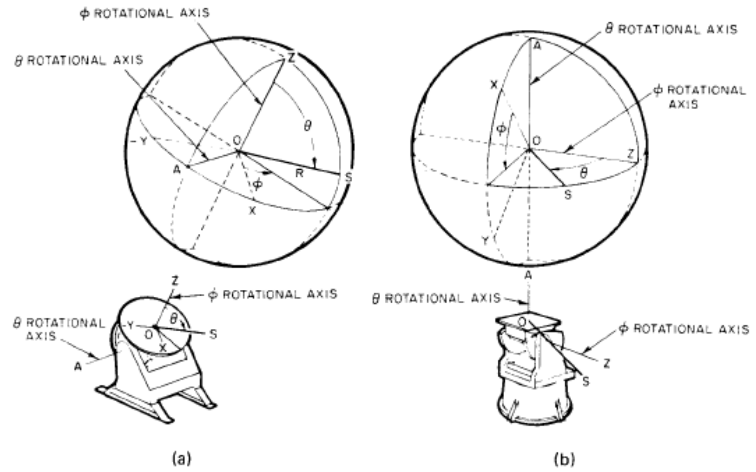

Figure 2.4: Standard positioner configurations and their spherical coordinate Systems

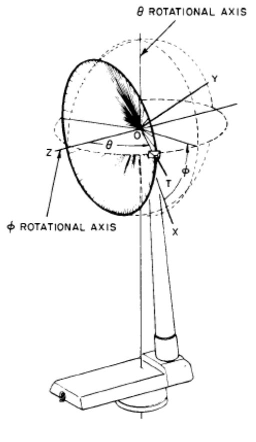

Figure 2.5: Model tower and its spherical coordinate system

2.3.1 Gain Measurements

The *gain* of an antenna is defined as the ratio of its maximum radiation intensity (power flow per unit area) to the maximum radiation intensity of a standard antenna, both antennas being equally energized. In the past, this standard antenna has been a half-wave dipole, but in microwave measurements it has been replaced by a hypothetical antenna which radiates uniformly in all directions, i.e., an isotropic radiator. When the gain is compared to that of this isotropic radiator, it is defined as the absolute gain of the antenna.

Two general methods of determining the gain of microwave antennas are possible: *Absolute Gain Measurements*, and *Gain Comparison Measurements*. The former is usually difficult to perform, so that the one more commonly employed is that of measuring the gain relative to some accurately calibrated secondary standard. The absolute gain of this standard antenna, however, must be accurately known, and it is therefore generally determined by the absolute-gain-measuring.

Absolute Gain Measurements

Absolute-gain measurements are based upon the Friis transmission formula (see 2.5), which states that for a two-antenna system the power received at a matched load connected to the receiving antenna is given by

$$P_r \quad = \quad P_t G_t G_r \left(\frac{\lambda}{4\pi r} \right)^2 \tag{2.24}$$

where P_r is the power received, P_t is the power accepted by the transmitting antenna, G_t is the power gain of the transmitting antenna, and G_r

is the power gain of the receiving antenna. This form of the transmission formula implicitly assumes that the antennas are polarization matched for their prescribed orientations and that the separation between the antennas is such that farfield conditions is fulfilled.

The Friis transmission formula can be written in logarithmic form, from which the sum of the gains, in decibels, of the two antennas can be written as:

$$(G_t)_{\mathrm{dB}} + (G_r)_{\mathrm{dB}} = 20\log_{10}\left(\frac{4\pi r}{\lambda}\right) + 10\log_{10}\left(\frac{P_r}{P_t}\right) \tag{2.25}$$

If the two antennas are identical, it follows that their gains are equal so that

$$(G_t)_{\mathrm{dB}} = (G_r)_{\mathrm{dB}} = \frac{1}{2}\left[20\log_{10}\left(\frac{4\pi r}{\lambda}\right) + 10\log_{10}\left(\frac{P_r}{P_t}\right)\right] \tag{2.26}$$

The procedure in determining the power gain of the antennas is to measure r, λ, and the ratio $\frac{P_r}{P_t}$, and then compute the gain of the antenna. Since two identical antennas are required, this method is referred to as *the two-antenna method.* If two antennas are not identical, a third antenna is required to determine the gains. For *the three-antenna method* three sets of measurements are performed using all combinations of three antennas. Three equations, one for each combination, can be written, and each takes the form of (2.24).

The instrumentation required for the measurement of gain using the two-antenna or three-antenna methods shall be highly stable with the source producing a single sinusoidal frequency. it is fundamental calibrate the coupling network between the source and the transmitting antenna so that the power measured at the transmit test point can be accurately related to the power into transmitting antenna. Then all components of the system are impedance matched using tuners. Finally the two antennas are separated so that far-field conditions prevail and boresighted so that they are properly aligned and oriented. If the gains of broad-band antennas are to be measured, it may be necessary to use the swept-frequency technique.[20] Both the two-antenna and the three-antenna methods can be employed.

Gain Comparison Measurements

The gain-comparison measurement, also know the gain-transfer measurement, is the method most commonly used to measure the gain of a test antenna. This technique utilizes a gain standard to determine absolute gain and require two sets of measurement. The electromagnetic horn is commonly used for this purpose because of its basic simplicity, reliability, and desirable broad-band impedance characteristics, and because its gain can be calculated from the physical dimensions.

Initially the test antenna is illuminated by a plane wave which is polarization matched to it, and the received power P_T is measured into a matched load, later the test antenna is replaced by a gain standard, leaving all other conditions unchanged, and the receiver power P_S is recorded. From the Friis transmission formula it can be shown that the power gain $(G_T)_{\mathrm{dB}}$ of the test antenna, in decibels, is given by:

$$(G_T)_{\mathrm{dB}} = (G_S)_{\mathrm{dB}} + 10\log_{10}\left(\frac{P_T}{P_S}\right) \tag{2.27}$$

where $(G_s)_{\mathrm{dB}}$ is the power gain of the gain-standard antenna.

One method of achieving this exchange between test and gain-standard antennas is to mount the two antennas back to back on either

---

[20] Standard, “IEEE Standard Test Procedures for Antennas”, section 7.4.

side of the axis of an azimuth positioner. With this configuration the antennas can be switched by a 180° rotation of the positioner. Usually absorbing material is required immediately behind the gain standard to reduce reflections in its vicinity which might perturb the illuminating field. Swept-frequency gain-transfer measurements can be performed for testing broad-band antennas. The procedure is essentially the same as that for the swept-frequency absolute-gain measurement, only that the measurement is repeated with the test antenna and the gain standard.

If the test antenna is circularly o elliptically polarized, gain measurements can be accomplished by two different methods. One approach is to design a standard gain antenna whit circular or elliptical polarization. In general, the power gains of circularly and elliptically polarized test antennas are measured with the use of linearly polarized gain standards. This is valid because the total power of the wave radiated by an antenna can be separated into two orthogonal linearly polarized components. A single linearly polarized gain standard can be employed and rotated 90° to achieve both vertical and horizontal polarizations. Thus the total gain of the circularly or elliptically polarized test antenna can be written as:

$$(G_T)_{\mathrm{dB}} = 10\log_{10}\left(\frac{G_{TV}}{G_{TH}}\right) \tag{2.28}$$

where $(G_{TV})_{\mathrm{dB}}$ and $(G_{TH})_{\mathrm{dB}}$ are the partial power gains with respect to vertical linear polarization and horizontal linear polarization, respectively.

2.3.2 Polarization Measurements

In similar manner as for a plane wave, the polarization of an antenna is defined as the curve described by the tip of the instantaneous electric

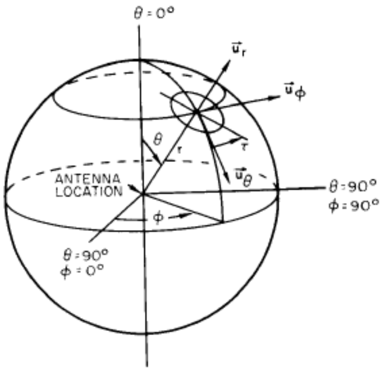

Figure 2.6: Polarization Ellipse in Relation to Antenna Coordinate System

field radiated by the antenna in a plane perpendicular to the direction of propagation. This locus is usually an ellipse. Elliptical polarization is characterized by the AR[21] of the polarization ellipse, the sense of rotation, and the spatial orientation of the ellipse with respect to a reference direction in the plane containing the ellipse, the tilt angle[22]. For most antenna-pattern-measurement situations it is convenient to establish a local coordinate system in a plane perpendicular to a line drawn between the test antenna and the source antenna, the horizontal axis is usually chosen as the reference direction. Since an antenna usually has a spherical coordinate system associated with it, its polarization in a direction (θ, ϕ) can be illustrated with respect to the coordinate system, as shown figure 2.6.

Also, in order to be consistent with the definition of antenna polarization, the local coordinate system associated with each of the waves

---

[21] see 2.1

[22] see 2.22

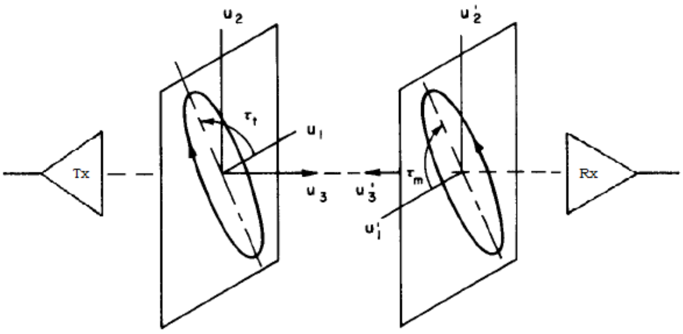

Figure 2.7: Relation between polarization properties of an antenna when transmitting and receiving

is oriented so that one of the coordinates is in the direction of propagation. As a result the tilt angles for the two polarization ellipses, which are measured according to a right-hand rule, are different. As shown in figure 2.7, if τ_t is the tilt angle for the ellipse described by E_t, which is polarized matched to the receiving antenna, then the one described by E_r will be $\tau_r = 180° - \tau_t$.

Various techniques are used to determine the polarization of microwave antennas, these can be classified into three categories: *Absolute Methods*, which yield complete polarization information and require no a prior polarization knowledge or no polarization standard; *Comparison Methods*, which yield complete polarization information, but require a polarization standard for comparison, and those that yield partial information about the antennas polarization properties.
The following methods may be employed to measure polarization:

- polarization-pattern method

- rotating-source method
- multiple-amplitude-component method
- phase-amplitude method

The *polarization-pattern method* may be employed to determine the tilt angle and the magnitude of the axial ratio, but it does not determine the sense of polarization. For this measurement the antenna under test can be used in either the receive or the transmit mode. If it is used in the transmit mode, the method consists of the measurement of the relative voltage response $|V|$ of a dipole, or other linearly polarized probe antenna, while it is rotated in a plane normal to the direction of the incident field. The pattern form a figure-eight, as show in figure 2.8, where ψ is the rotation angle of the probe relative to a reference direction. The magnitude $|V|$, when plotted as a function of the tilt angle τ_r of the receiving polarization of the linearly polarized probe antenna, is called a polarization pattern. For an elliptical polarized test antenna, the null of the figure-eight are filled to polarization curve (figure 2.8).
The polarization pattern is tangent with the polarization ellipse of the field at the ends of the major and minor axes. Hence the magnitude of the axial ratio and the tilt angle of the incident wave are determined. The polarization pattern will be a circle if the test antenna is circularly polarized.

The axial ratio (and not the sense of polarization or the tilt angle) can be determined as a function of direction by using the *rotating-source method.* The method consists of continuously rotating a linearly polarized source antenna while the direction of observation of the test antenna is changed. A pattern of an elliptically polarized antenna obtained by the

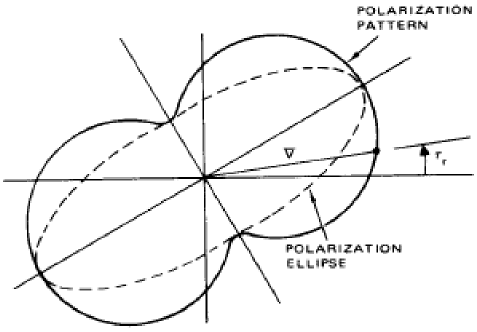

Figure 2.8: Continuously scanned polarization pattern as a function of angle θ

rotating source method is shown in figure 2.9. If the amplitude variations are plotted in decibels, the axial ratio, also in decibels, for any direction in space that is recorded on the pattern is the width of the envelope of the excursions.

The sense of rotation can be determined by performing auxiliary measurements. One method requires that the response of two circularly polarized antenna of opposite hand, one responsive to clockwise and the other to counterclockwise rotation, be compared. The sense of rotation corresponds to the sense of polarization of the antenna with the more intense response.

Another technique is the *multiple-amplitude-component method*. The test antenna polarization can be determined from the magnitudes of the responses of four sampling antenna having different, but known, polarizations from the following six choices: horizontal or vertical linear polarization, 45° or 135° linear polarization, and right-hand or left-hand circular polarization. Usually it is more convenient to measure the magnitudes

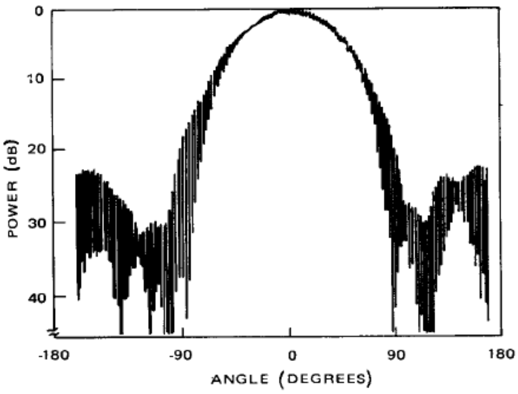

Figure 2.9: Continuously scanned polarization pattern as a function of angle θ

of the linear, diagonal linear, and circular polarization ratios. The axial ratio and the sense of polarization are determined from circular polarization ratio since $AR = \frac{XPD+1}{XPD-1}$. If the AR is positive the sense is right handed while it is negative the sense is left handed.

In the *phase-amplitude method* a dual-polarized receiving antenna, linear or circular polarized, is used to sample the field of the antenna under test which is, in this case, used as a transmitting antenna. The outputs of the receiver will be the magnitudes of the responses for each of the polarizations of the sampling antenna and their relative phases. If the two polarizations are orthogonal, the complex polarization ratio can be obtained.

2.3.3 Anechoic Chamber

An anechoic chamber is a room designed to completely absorb reflections of either sound or electromagnetic waves. They are also insulated from exterior sources of noise. The combination of both aspects means they simulate a quiet open-space of infinite dimension, which is useful when exterior influences would otherwise give false results.

The RF anechoic chamber is typically used to house the equipment for performing measurements of antenna radiation patterns, electromagnetic compatibility (EMC) and radar cross section measurements. Testing can be conducted on full-scale objects, including aircraft, or on scale models where the wavelength of the measuring radiation is scaled in direct proportion to the target size.

The interior surfaces of the RF anechoic chamber are covered with radiation absorbent material (RAM). One of the most effective types of RAM comprises arrays of pyramid shaped pieces, each of which is constructed from a suitably lossy material. To work effectively, all internal surfaces of the anechoic chamber must be entirely covered with RAM.

Typically pyramidal RAM will comprise a rubberized foam material impregnated with controlled mixtures of carbon and iron, they are installed with the tips pointing inward to the chamber.

The length from base to tip of the pyramid structure is chosen based on the lowest expected frequency and the amount of absorption required. For low frequency damping, this distance is about 60 cm, while high frequency panels are as short as 7-10 cm.

Also, the pyramid shapes are cut at angles that maximize the number of bounces a wave makes within the structure. With each bounce, the wave loses energy to the foam material and thus exits with lower signal strength.

There are two basic types of anechoic chambers, the rectangular and the tapered types.
The *rectangular anechoic chamber* is usually designed to simulate free-space conditions. Even though the sidewalls, floor, and ceiling are covered with absorbing material, significant specular reflections can occur from these surfaces, especially for the case of large angles of incidence. One precaution that can be taken is to limit the angles of incidence to those for which the reflected energy is below the level consistent with the accuracy required for the measurements to be made in the chamber. Often, for high-quality absorbers, this limit is taken to be a range of incidence angles of 0° to 70° (as measured from the normal to the wall).[23]

The *tapered anechoic chamber* is designed in the shape of a pyramidal horn that tapers from the small source end to a large rectangular test region. This type of anechoic chamber has two modes of operation. At the lower end of the frequency band for which the chamber is designed it is possible to place the source antenna close enough to the apex of the tapered section so that the reflections from the sidewalls, which contribute directly to the field at the test antenna, occur fairly close to the source antenna. Using raytracing techniques, one can show that for a properly located source antenna there is little change in the phase difference between the direct-path and the reflected-path rays at any point in the test region of the tapered chamber. The net effect is that these rays add vectorially in such a manner as to produce a slowly varying spatial interference pattern and hence a relatively smooth illumination amplitude in the test region of the chamber. As the frequency of oper-

---

[23] Standard, “IEEE Standard Test Procedures for Antennas”, section 4.5.4 pag. 17.

ation is increased, it becomes increasingly difficult to place the source antenna near enough to the apex. A higher gain source antenna is used in order to suppress reflections when this occurs. It is moved away from the apex, and the chamber is then used in the free-space mode similar to the rectangular chamber.[24]

---

[24] Standard, "IEEE Standard Test Procedures for Antennas", section 4.5.4 pag. 18.

Chapter 3

Circularly Polarized Antenna

In this section is reported the design, develop, manufacture and experimentally validate two simple and efficient solutions for the antenna operating at 5.8 GHz. Either structures are patch antenna which the circular polarization is obtained exciting two orthogonal modes with equal magnitudes and in phase quadrature. The antennas have been optimized by means of the electromagnetic simulator in order to achieve circular polarization with Axial Ratio lower than 3 dB at the operating frequency.

3.1 Dedicated Short-Range Communications Overview

The Dedicated Short-Range Communications (DSRC) is a suite of wireless standards based on the WiFi architecture, developed mainly by the Institute of Electrical and Electronic Engineers (IEEE), operating in radio frequency in the 5.725 GHz to 5.875 GHz Industrial, Scientific and Medical (ISM) band, for communications between Vehicle-to-Vehicle (V2V) e Vehicle-to-Infrastructure (V2I).

Dedicated Short-Range Communications Systems provide a high-speed radio link between Road Side Equipment (RSE), a fixed unit placed on a road infrastructure, and On-Board Equipment/Unit (OBE/OBU), a mobile unit placed inside the vehicle, within a small communication range, up to 1000 meters in optimal weather condition.

In Europe the EN12253 standard[1] specifies the requirements for the communication between RSE and OBU at 5.8 GHz and the OBU antenna features as applicable in the Road Transport and Traffic Telematics (RTTT). The OBU antenna should have a 20 MHz bandwidth (5.795-5.815 GHz) an unidirectional radiation pattern with a main lob width of 70° in the vertical plane with the angular EIRP mask suppression of 15 dB, a Cross Polarization Discrimination (XPD) greater than 10 dB in boresight direction and greater than 6 dB within the -3 dB area.

In recent years the OBU market for Electronic Toll Collection (ETC) is rapidly increasing and spreading to several countries, and can be estimated around 1ML/year due to the large number of OBU devices required. Small size and low cost are the main features for commercially attractive OBU implementation.

For these reasons in the next paragraphs will show two simple and efficient solutions suitable for a OBU antenna of a DSRC system.

---

[1] *European Standard EN 12253, Comité Européen de Normalisation (CEN), Jul., 2004.*

3.2 Cross-Slot Coupled Patch Antenna

In this section we will show the study and the experimental characterization of double-layer patch antenna in which the coupling between the feed and the radiating patch is realized through a cross-shaped aperture in the ground plane placed between two layers laminate with the same electromagnetic properties. Appropriately dimensioning the slot sizes and patch lengths left circular polarization is obtained.

3.2.1 Antenna Layout

The first antenna structure is designed and realized on Arlon 450, a substrate with relative permittivity ϵ_r= 4.5 and $\tan\delta = 0.0035$. Arlon 450 represents a good alternative to standard FR4, since it has the same permittivity with a very stable behavior at higher frequencies and a better loss tangent. The proposed configuration is a slot-coupled patch antenna, the two substrates have the same permittivity with different height $h_1 = 0.78$ mm and $h_2 = 1.57$ mm, respectively. The antenna has been designed with total size of 40mm × 40mm × 2.455mm to achieve circular polarization with Axial Ratio lower than 3 dB at 5.8 GHz. The layout antenna is shown in figure 3.1 and the parameters are listed in table 3.1

The 50 Ω feeding microstrip line is placed on the 0.78 mm thick layer, while the radiating patch is realized on the 1.57 mm layer. The microstrip feed line and the slotted ground plane are etched on the opposite sides of the first substrate and the feeding structure (strip and slotted ground plane) is assembled to be centered below to an almost square patch printed on the second substrate. The common ground plane has a

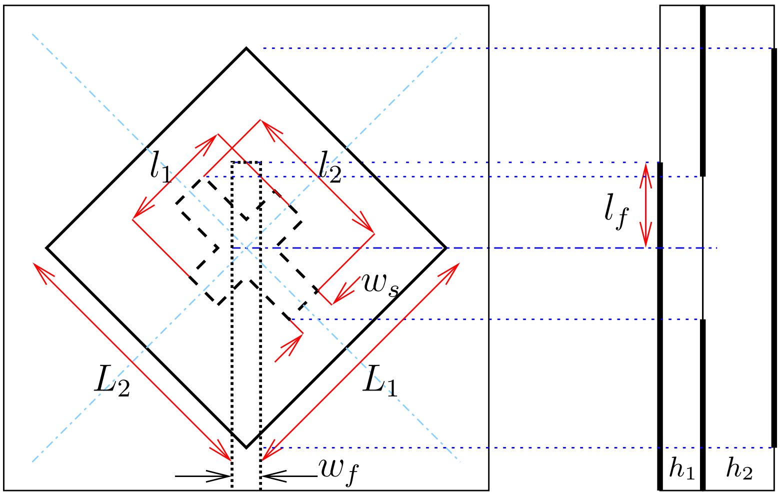

Figure 3.1: Antenna layout front and side view. A continuous line is used for the patch, a dashed line for slot in the ground plane, and a dotted line for the 50 Ω feeding microstrip.

cross slot with slightly unequal slot lengths and 45° inclined with respect to the microstrip feed line.

It is known that the resonant frequency of the microstrip patch decreases with the increasing of the coupling slot length,[2] by carefully adjusting the lengths of the two arms of the cross-slot the first two resonant frequencies of the patch can be achieved with near-equal amplitudes and in phase quadrature. Assuming for simplicity that the patch is perfectly square the resonant frequency of the resonant mode in the direction perpendicular to the longer slot will be slightly lower than that of the resonant mode in the direction perpendicular to the shorter slot, con-

---

[2] Sullivan and Schaubert, "Analysis of an aperture coupled microstrip antenna".

Table 3.1: Coupled Cross-slot Parameters

Parameter	**Description**	**Dimension [mm]**
S	ground plane size	40
ϵ_r	permittivity	4.5
$\tan\delta$	loss tangent	0.0035
h_1	down substrate height	0.78
h_2	upper substrate height	0.78
h_m	metal height	0.035
L_1	patch size	9.85
L_2	patch size	10.4
l_1	slot length	5.4
l_2	slot length	5.8
w_s	slots width	1.7
w_f	feed length	1.5
l_f	stub length	3.8

sequently when $l_1 > l_2$ a right-hand can be obtained, viceversa, when $l_1 < l_2$ a left-hand CP operation can be achieved.

For ease of fabrication and assembly, the same slotted ground plane has been replicated on the 1.57 mm thick substrate, but the two grounds electrically form a single metal layer. To this regard, for an industrial series production the real final layer stack-up should be considered for fine tuning of CP and some correction steps should be carried out to correctly consider epoxy.

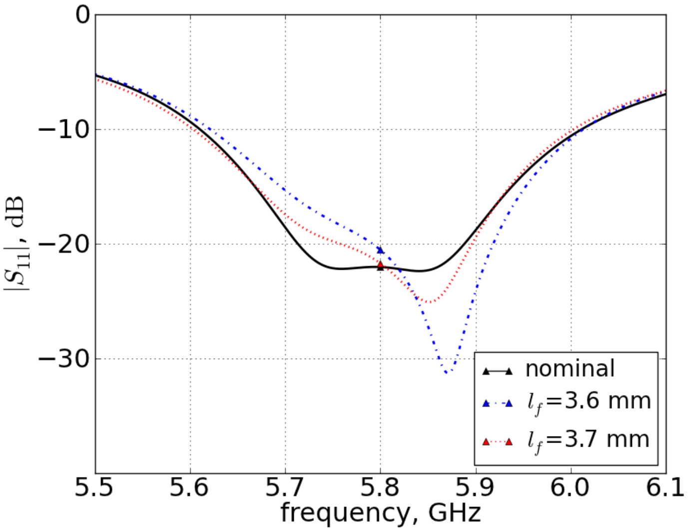

Figure 3.2: Simulated $|S_{11}|$ to 100μm variation in the stub length l_f

3.2.2 Antenna Optimization

Different patch lengths, L_1 and L_2, and slot lengths, l_1 and l_2, are used to balance the mode amplitudes as well as to control their phase difference in order to achieve circular polarization at 5.8 GHz.[3] The stub length, l_f, can be adjusted to match the antenna, figure 3.2 show how a 100 μm variation of l_f influences the $|S_{11}|$.

The operation frequency is determined by patch size. Figure 3.3 show how a 50 μm differential or common mode variation of L_1 and L_2 influences the $|S_{11}|$.

---

[3] The antenna optimization was carried out by time-domain finite-element EM simulation software CST Microwave Studio (CST MWS).

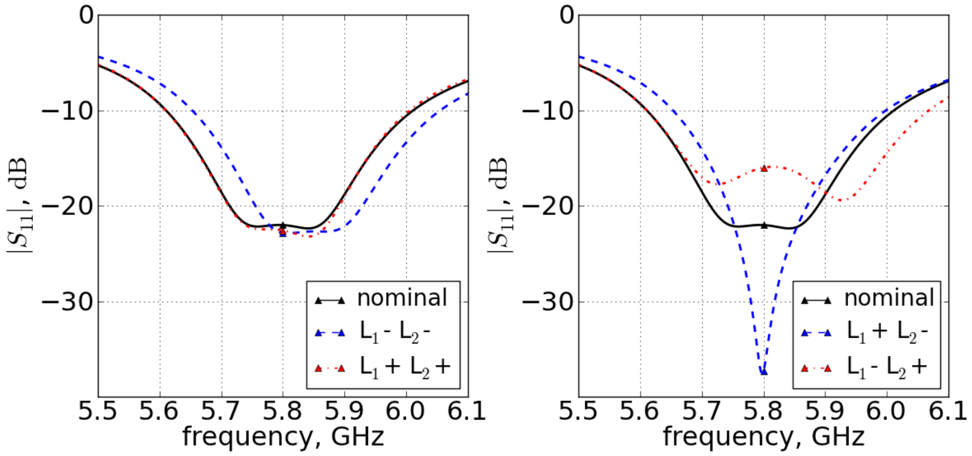

(a) (b)

Figure 3.3: Simulated $|S_{11}|$ to 50μm increase/decrease in the patch dimensions L$_1$ and L$_2$: (a) common mode; (b) differential mode

3.2.3 Experimental Result

To easily mount a SMA-connector it was decided to increase the 0.78 mm thick substrate of 2 cm along the $\hat{y}$-axis, thus achieving a layout with total size of 40×60 mm. In figure 3.4 it is possible to see the small size prototype antenna before assembly realized by photolithography process.

The measured and simulated S-parameters and Input Impedance are shown in Figure 3.5 *a* and *b* respectively, where it is possible to observe that the realized antenna is well matched from 5.6 GHz to 6 GHz for a 6.89% impedance bandwidth. The simulated curves are reported for both the realized 40×60 prototype and the 40×40 reference design.

The experimental characterization of the coupled cross-slot antenna was performed in anechoic chamber (see 2.3.3).

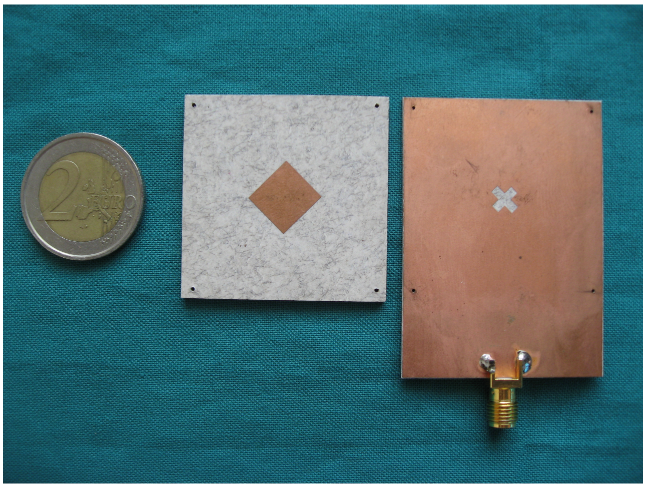

Figure 3.4: Cross-slot prototype antenna before assembly

The gain and polarization patterns of the test antenna were measured using a linearly polarized source produced by an Horn antenna. A LHCP gain of about 5.52 dBc was estimated by Gain Comparison Method replaced the antenna under test with a calibrate horn antenna with standard gain of G$_{std}$=15.4 dBi (see 2.3.1). The absolute gain of the test antenna is determined from the difference in the measured power level[4] plus a 3 dB increase that represent the difference in power received by a circular isotropic antenna when these are illuminated by a linear polarization signal.

In Figure 3.6*a* are reported the measured and simulated gain pattern for a linearly polarized incident wave along different directions. In the ideal case of circular polarization (AR=0 dB) all the angular gain patterns should be superimposed. Here it is possible to see that the exper-

---

[4] see equation 2.28

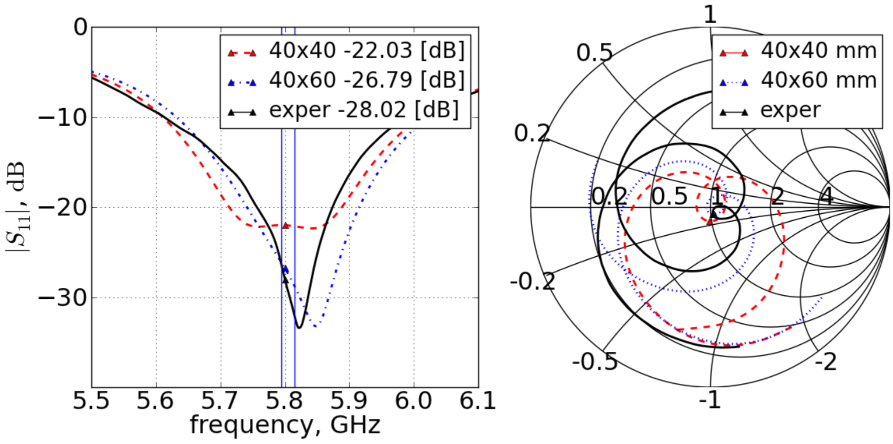

(a) (b)

Figure 3.5: Measured and simulated impedance bandwidths: (a) Experimental and simulated $|S_{11}|$. Vertical lines show the DSRC band; (b) Input impedance on a Smith Chart

imentally measured patterns are closer than those simulated, witnessing a good CP.

Figure 3.6*b* shows the experimentally measured polarization ellipse in the boresight direction at 5.8 GHz. A linear polarized incident field is considered and the detected signal is plotted versus the the OBU antenna rotation from 0° to 180°. From the latter figure it is possible to extrapolate an Axial Ratio of about 1.7 dB, which corresponds to an XPD of about 20 dB.

In order to estimate the CP frequency bandwidth the boresight normalized gain vs. frequency is plotted in Figure 3.7 with different relative orientation between the antenna and the linearly polarized incident field. Here it is possible to check an axial ratio value of 1.7 dB at the operating

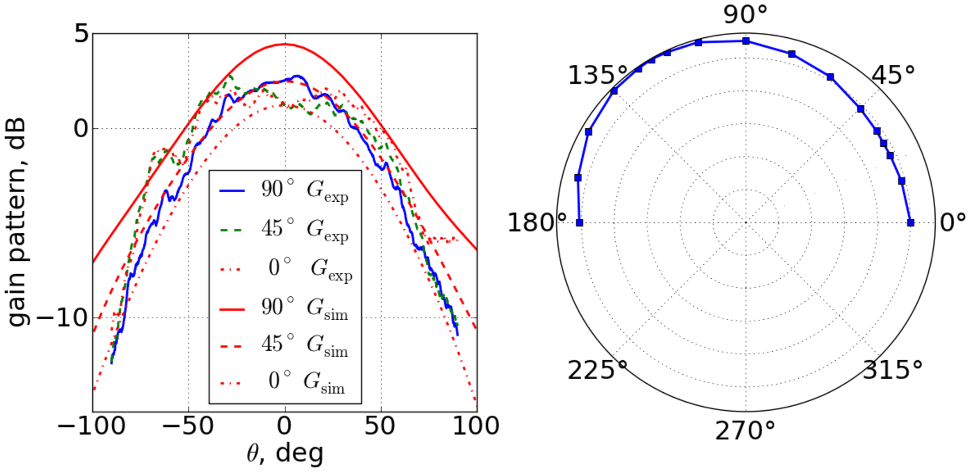

(a) (b)

Figure 3.6: Farfield measurements: (a) *Measured and simulated gain pattern for a linearly-polarized incident electric field at 0°, 45° and 90°. The 3 dB polarization loss are not compensated*; (b) *Measured polarization ellipse in the boresight direction at 5.8 GHz.*

frequency and a further decrease to about 5.83 GHz.

The results returned from the experimental measurements meet the standard requirements and are obtained with a very compact design which is required for a small device suitable for a OBU in an Electronic Toll Collection system.

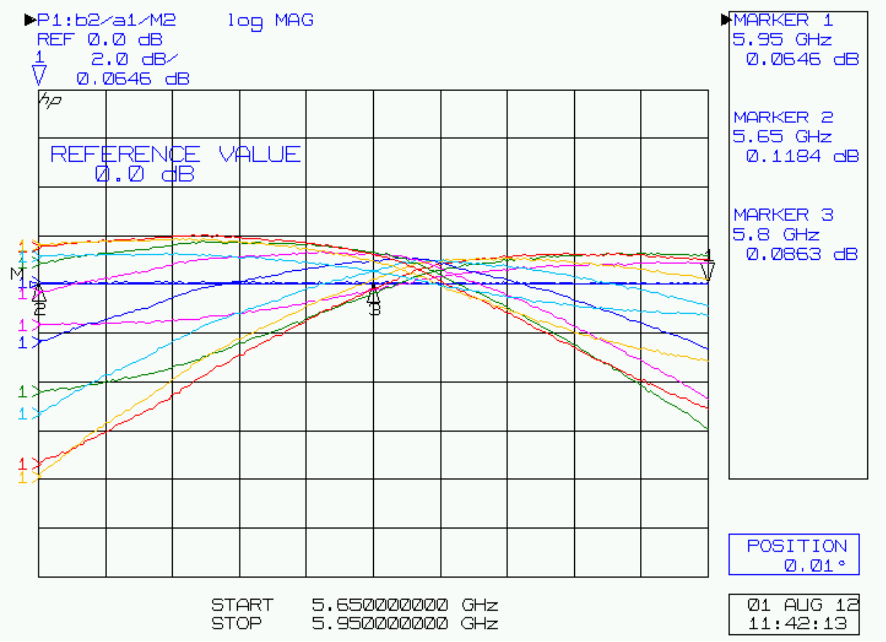

Figure 3.7: Boresight gain. The curves are normalized to a reference one.

3.3 Elliptical-Slotted Patch Antenna

In this section will be shown another CP antenna layout which consist of a circular disc slotted by a concentric elliptical cut with coaxial feed, always operating a 5.8 GHz e design su FR4 epoxy. Compared with the structure described in the previous section, this antenna has the advantage of being one-layer and therefore of simpler fabrication as well as less expensive.

3.3.1 Antenna Layout

The proposed circularly polarized antenna is designed and realized on standard FR4 with a nominal relative permittivity $\epsilon_r = 4.6$ and $\tan\delta = 0.018$. The antenna layout is shown in figure 3.8 and geometric parameters are listed in table 3.2.

The proposed configuration is a circular patch antenna with an elliptical central slot on the patch. The feeding probe is the inner conductor of a 50 Ω coaxial cable which through the substrate is connected to the patch along the diagonal at $(x_f, y_f) = (1.8, 1.75)$ mm.

A well known feature of the proposed structure is the ability to change the right- into left- circular polarization and viceversa simply mirroring the feed point about one axis of the ellipse. Figure 3.8 shows the layout to obtaining left-hand circular polarization, the right-hand operation can be achieved by moving the feed at $(x_f, y_f) = (-1.8, 1.75)$ mm.[5]

---

[5] Balanis, *Antenna theory*, pag. 767.

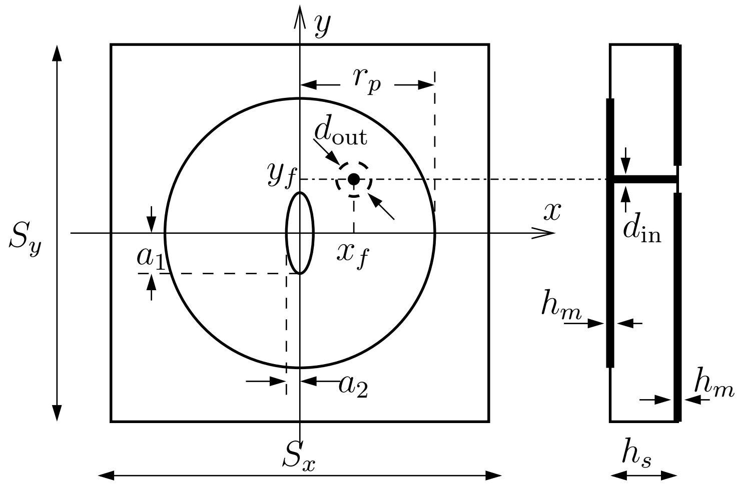

Figure 3.8: Antenna layout: front and side view. A continuous line is used for the patch, a dashed line for guard ring on the ground plane

3.3.2 Antenna Optimization

Adjusting the lengths of major and minor lengths, a_1 and a_2 respectively, the fundamental resonant frequency of the circular patch can be split into two near-degenerate resonant modes in order to achieve circular polarization with Axial Ratio lower than 3 dB at 5.8 GHz.[6] Figure 3.9 shows how a 100μm variation of semi-axis influences the AR. The ground plane size indirectly affects the AR, as shown in Figure 3.10, while the corresponding radiation efficiency and gain are not influenced significantly, as shown Table 3.3.

In order to facilitate the subsequent activities of experimental measurement and integration, it was decided to realize the prototype with larger dimensions, without further optimization.

---

[6] The antenna optimization was carried out by FEM simulator HFSS v.15

Table 3.2: Elliptical-slotted Antenna Parameters

Parameter	**Description**	**Dimension [mm]**
$Sx = Sy$	ground dimension	25
ϵ_r	permittivity	4.1
$\tan\delta$	loss tangent	0.018
h_s	substrate height	1.55
h_m	metal height	0.035
r_p	patch radius	6.75
a_1	major axes	3.2
a_2	minor axes	0.5
d_{in}	inner probe radius	0.7
d_{out}	outside probe radius	2.34
x_f	$\hat{x}$ probe	1.8
y_f	$\hat{y}$ probe	1.75

Table 3.3: Farfield parameters for a variation of the ground plane dimension

Sx=Sy [mm]	**AR [dB]**	**Gain [db]**	**RE [mag %]**
40	1.44	4.77	66.26
30	0.71	4.8	67.35
25	0.4	4.77	65.32

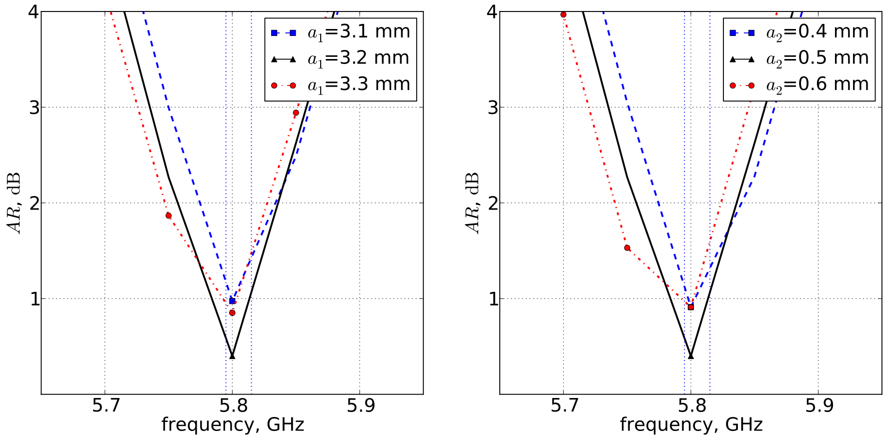

(a) (b)

Figure 3.9: Simulated AR; vertical lines show the DSRC band: (a) variation of major axis; (b) variation of minor axis

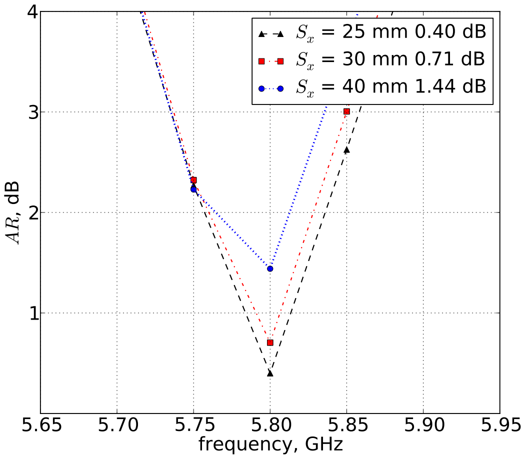

Figure 3.10: Simulated AR for variation of the ground plane dimension

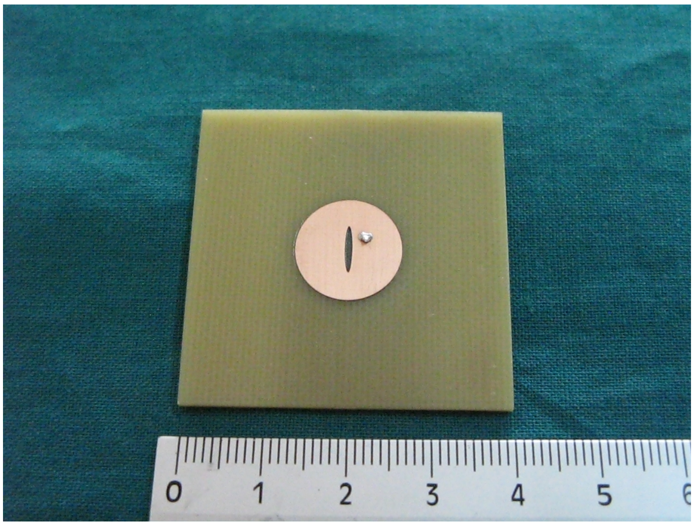

Figure 3.11: Elliptical-slot L-prototype antenna

3.3.3 Experimental Result

The antenna prototype was realized by CNC milling machine with a radius tip equal to 0.25 mm, it is show in figure 3.11.

In Figure 3.12 are shown both measured and simulated VSWR and S-parameters on Smith Chart. As it can be see that the realized antenna is well matched from 5.6 GHz to 6.05 GHz for a 7.75% impedance bandwidth.

The same figure also reports the experimental trace belonging to a geometrically-identical prototype with a mirrored feed operating in RHCP. Theoretically the two L- and R- antenna, differing only for polarization of the radiated field, should have identical VSWR; the small differences between the two traces are due to manufacturing tolerances.

In order to characterize the polarization state of the prototype was

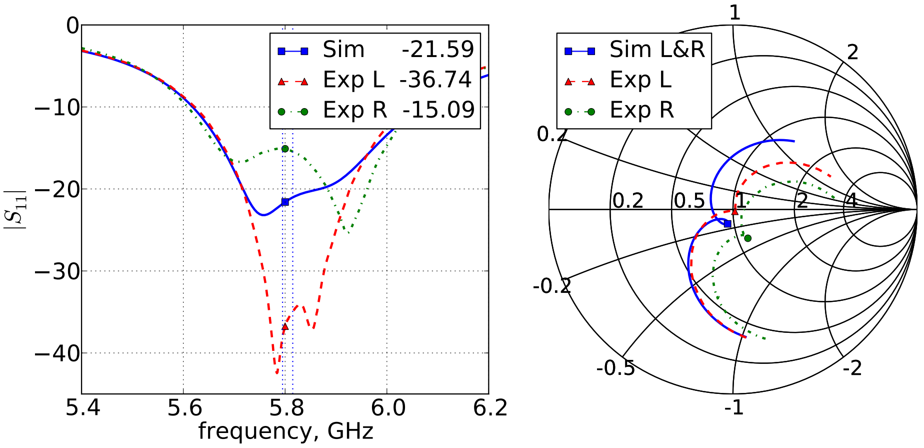

(a) (b)

Figure 3.12: Measured and simulated impedance bandwidth: (a) Experimental and simulated VSWR (vertical lines show the DSRC band); (b) Input impedance on a Smith Chart

used a non-canonical method of polarization measurement because in general it is not economically feasible to get a dual-polarized antenna with known pure polarizations. Therefore to experimentally evaluate the XPD the check pair of two identical symmetrically fed prototypes were illuminated by a same wideband truncated conical LHCP antenna. The ratio of the power received by the L- and R- prototypes, in the same illumination conditions, allows us to estimate the Cross Polarization Discrimination[7].

In Figure 3.13 the S_{12} vs. frequency is shown for a L- an R-prototype using a LHCP incident wave. At 5.8 GHz we achieve an XPD of about

---

[7] see section 2.3.2

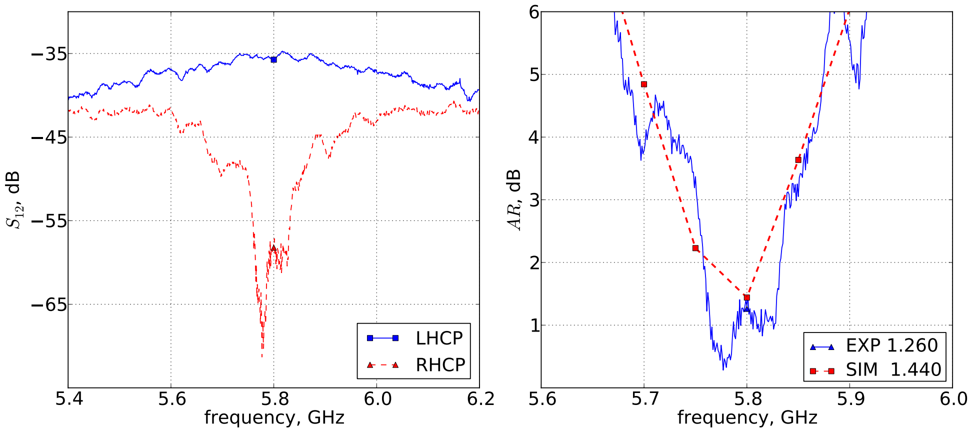

(a) (b)

Figure 3.13: Experimental measurements: (a) S_{12} for a LHCP incident wave and the LHCP/RHCP antenna prototypes (continuous and dashed line respectively); (b) AR versus frequency

22.5 dB, from which it is possible to derive an AR of 1.3 dB. This value is in good agreement with the polarization ellipse measured in the boresight direction at 5.8 GHz.

The polarization ellipse is shown in Figure 3.14 for a linearly polarized incident field, the detected signal is plotted versus the OBU antenna rotation from 0° to 180°. From the same figure it is possible to extrapolate an AR of about 1.45 dB.

The gain was calculated using a number of three identically polarized antennas by the Three-Antenna Method.[8]
The estimated gain is 4.68 dBc, slightly lower than the simulated value. To achieve this result you have performed all the possible combinations

---

[8] see section 2.3.1

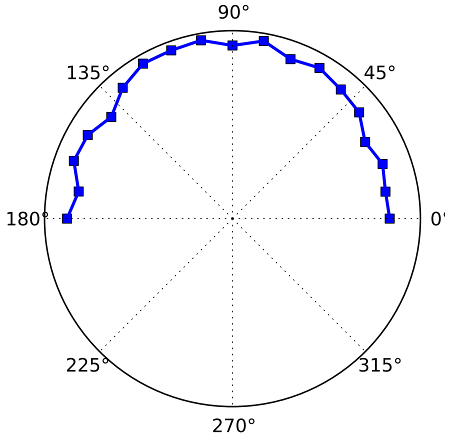

Figure 3.14: Measured polarization ellipse in the boresight direction at 5.8 GHz

between a wideband truncated conical LHCP antenna, the cross-slot coupled prototype characterized in the previous section and the L-prototype elliptical-slot.

The experimental characterization confirms that requirements imposed by the DSRC standards are fulfilled with a simple design being compact, monolithic, low-profile, low-cost and suitable for integration on a circuit board.

3.3.4 Technical Notes

To create a finite element mesh the HFSS electromagnetic simulator first divides all true surfaces into triangles. These triangulated surfaces are called *faceted surfaces* because a series of straight line segments represents each curved or planar surface.
For planar surfaces, the triangles lie exactly on the model faces; when an object's surface is non-planar, the faceted triangle faces lie a small distance from the object's true surface. This distance is called the *surface deviation*, and it is measured in the model's units. The surface deviation is greater near the triangle centers and less near the triangle vertices.
The normal of a curved surface is different depending on its location, but it is constant for each triangle (in this context, "normal" is defined as a line perpendicular to the surface). The angular difference between the normal of the curved surface and the corresponding mesh surface is called the *normal deviation* and is measured in degrees.
The aspect ratio of triangles used in planar surfaces is based on the ratio of circumscribed radius to the in-radius of the triangle. It is unity for an equilateral triangle and approaches infinity as the triangle becomes thinner.

In order to simulated curved surfaces more accurately, in our case patch and elliptical-slot, it was necessary to override default settings of the Maximum Surface Normal Deviation and Maximum Aspect Ratio. Modification surface approximation involves variations to initial mesh, with the resulting increase of the mesh size and greater consumption of CPU time and memory.

Chapter 4

High Impedance Surfaces

In recent years, the realization of *Artificial Magnetic Conductors* (AMCs), also known as *High Impedance Surfaces* (HISs), has been an active area of research as they can be used to improve the strength of the radiating fields, the gain and the directivity of antennas[1] and to reduce the global thickness of the low profile antennas [2].

HISs are typically fabricated as printed circuit boards, where the bottom side is a metal ground plane and the top contains an array (*elementary cell*) of small ($<< \lambda$) metal patch. By properly selecting periodicity and the geometry of the printed elements, it is possible to obtain an elevate surface impedance within a precise frequency band, up to the limit of perfect magnetic conductor.[3] The reflection phase is defined as the phase of the reflected electric field at the reflecting plane. It is relative

---

[1] Ayad et al., “Performances of low profile dipole antenna AMC-based surface using metamaterials structures”.

[2] The low profile design usually refers to the antenna structures whose overall height is less than one tenth of the wavelength at the operating frequency.

[3] An HIS can be characterized by its reflection

to the phase of the incident electric field at the reflecting plane. It is well known that a PEC has an 180° reflection phase for a normally incident plane wave and a PMC has a 0° reflection phase. In contrast, the typical reflection phase of the AMC surface decreases continuously from 180° to -180° as frequency increases.

In order to achieve good return loss and high efficiency, low profile antennas are generally made placing horizontal radiating element close to an AMC surface which is designed to exhibit a zero degree reflection phase frequency that coincides with the operating frequency of the antenna. Therefore, tuning the reflection phase characteristics of the proposed AMC structure is important. To accurately characterize the in-phase reflection coefficient, a finite element method (FEM) technique and appropriate boundary condition cab be used to analyze the proposed AMC structure (see 4.3.1).

Indeed it has been shown that the useful operational frequency band of an AMC structure is the frequency region inside which the AMC structure shows quadratic reflection phase (90° ± 45°).[4] This frequency range is defined as *input-match frequency region.*

The AMC surfaces are also effectively used to suppress surface waves from a metal interface over finite frequency band.[5] The air lossy-metal interface can support surface wave that propagate bound to the interface. On a finite ground plane, surface waves propagate until they reach an edge or corner, where they can radiate into free space. The result is a kind of multipath interference or speckle, which can be seen as ripples in

---

[4] Yang and Rahmat-Samii, “Reflection phase characterizations of the EBG ground plane for low profile wire antenna applications”.

[5] Sievenpiper et al., “High-impedance electromagnetic surfaces with a forbidden frequency band”.

the radiation pattern. If multiple antennas share the same ground plane, surface waves can cause unwanted mutual coupling.

In recent years, a polarization-dependent AMC structure was proposed using rectangular or square patch array to achieve polarization diversity antenna[6] . This complex artificial ground plane exhibits an in-phase reflection coefficient that allows to obtain a good return loss with a low profile configuration, while the polarization dependent feature of the reflection phase is used to convert the linear polarization of the single dipole to the circular polarization.

Several solution have been proposed to AMC surface: small metal bumps, corrugation and in recent years printed arrays of lumped circuit elements, as they are less expensive and easy to manufacture with standard photolithographic process.

4.1 Impedance Surface

As mentioned in the previous section, by incorporating a special texture on a conductor, it is possible to change its radio-frequency surface properties. In the limit where the period of the surface texture is much smaller than the wavelength, the structure can be described using an effective medium model, and its qualities can be summarized into a single parameter: *the impedance surface.*

The impedance surface is often modeled as a parallel resonant LC circuit, which act as a two-dimensional electric filter to block the flow of currents along the sheet and which can be tuned to exhibit high impedance over

---

[6] Yang and Rahmat-Samii, “A low profile single dipole antenna radiating circularly polarized waves”.

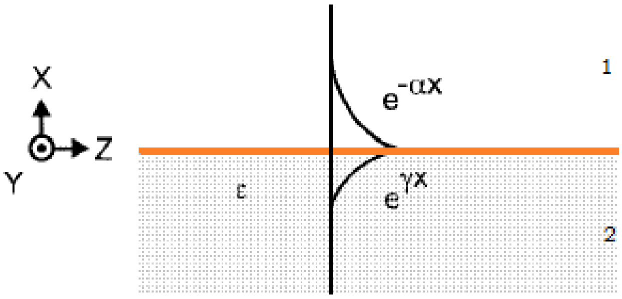

Figure 4.1: A surface wave on an interface between two dissimilar media

a predetermined frequency band. The impedance is very high near the resonance frequency $\omega_0 = \frac{1}{\sqrt{LC}}$.

As we will see below, in the frequency range where the surface impedance is very high, the tangential magnetic field is small, even with a large electric field, hence the name *magnetic conductor*.

To derive surface impedance for metal surface, begin by deriving the properties of surface waves on a general interface consists of two different materials having dielectric constant $\epsilon_1 = \epsilon_0\epsilon_{r1}$ and $\epsilon_2 = \epsilon_0\epsilon_{r2}$ respectively. The surface is in the yz plane, with material 1 extending in the positive x direction, and material 2 in the negative x direction, as shown in figure 4.1. Let us assume that for a wave to be bound to the surface, it decays in the positive x direction with decay constant α, and in the negative x direction with decay constant γ.

Consider a TM surface wave.

The field $\vec{E}$ in material 1 has the following form, within dependence $e^{j\omega t}$

is implicit:

$$\begin{aligned} E_x &= Ae^{-jkz-\alpha x} \\ E_y &= 0 \\ E_z &= Be^{-jkz-\alpha x} \end{aligned} \tag{4.1}$$

similarly in material 2:

$$\begin{aligned} E_x &= Ce^{-jkz+\gamma x} \\ E_y &= 0 \\ E_z &= De^{-jkz+\gamma x} \end{aligned} \tag{4.2}$$

where A, B, C, and D are constants.

By suitably combining the Maxwell's curl equations,

$$\vec{\nabla} \times \vec{B} = \frac{\epsilon_r}{c^2}\frac{\partial \vec{E}}{\partial t} \tag{4.3}$$

$$\vec{\nabla} \times \vec{E} = \frac{\partial \vec{E}}{\partial t} \tag{4.4}$$

we obtain:

$$\vec{\nabla} \times \vec{\nabla} \times \vec{E} = -\epsilon_r \frac{\omega^2}{c^2}\frac{\partial^2 \vec{E}}{\partial t^2} \tag{4.5}$$

bearing in mind that the y derivative of the electric field is zero, we have:

$$\hat{x}(\frac{-\partial^2 \vec{E}_x}{\partial z^2} + \frac{\partial^2 \vec{E}_z}{\partial x \partial z}) + \hat{z}(\frac{\partial^2 \vec{E}_x}{\partial x \partial z} - \frac{\partial^2 \vec{E}_z}{\partial x^2}) = \epsilon_r \frac{\omega^2}{c^2}(\hat{x}E_x + \hat{z}E_z) \tag{4.6}$$

Substituting equations (4.1) we obtain equations for the fields above the surface

$$\begin{aligned} k^2 A + jk\alpha B &= \epsilon_{r1}\frac{\omega^2}{c^2}A \\ jk\alpha A - \alpha^2 B &= \epsilon_{r1}\frac{\omega^2}{c^2}B \end{aligned} \tag{4.7}$$

Similarly, by inserting equation (4.2) into equation (4.6), we obtain equations for the fields below the surface:

$$\begin{aligned} k^2C - jk\gamma D &= \epsilon_{r2}\frac{\omega^2}{c^2}C \\ -jk\gamma C - \gamma^2 D &= \epsilon_{r2}\frac{\omega^2}{c^2}D \end{aligned} \tag{4.8}$$

By imposing the boundary condition at the interface for the tangential electric field and the normal electric we have:

$$A = C \tag{4.9}$$

$$\epsilon_{r1}B = \epsilon_{r2}D \tag{4.10}$$

combining equations (4.7), (4.8) with the (4.9), (4.10) we obtain a non-trivial solution for EM field where k, α and γ are:

$$k = \sqrt{\frac{\epsilon_{r1}\epsilon_{r2}}{\epsilon_{r1}+\epsilon_{r2}}}\frac{\omega}{c} \tag{4.11}$$

$$\alpha = \sqrt{\frac{-\epsilon_{r1}^2}{\epsilon_{r1}+\epsilon_{r2}}}\frac{\omega}{c} \tag{4.12}$$

$$\gamma = \sqrt{\frac{-\epsilon_{r2}^2}{\epsilon_{r1}+\epsilon_{r2}}}\frac{\omega}{c} \tag{4.13}$$

These equations describe surface waves on a general interface between two dissimilar dielectric materials.

For simplicity, assume that one of the materials is free space, let us

$\epsilon_{r2} = 1$, we obtain the following results:

$$k = \sqrt{\frac{\epsilon_r}{1+\epsilon_r}}\frac{\omega}{c} \tag{4.14}$$

$$\alpha = \sqrt{\frac{-1}{1+\epsilon_r}}\frac{\omega}{c} \tag{4.15}$$

$$\gamma = \sqrt{\frac{-\epsilon_r^2}{1+\epsilon_r}}\frac{\omega}{c} \tag{4.16}$$

From these equations, it can be seen that TM surface waves do not exist on dielectric materials. If ϵ_r is positive, then α and γ are imaginary, and the waves do not decay with distance from the surface; they are simply plane waves propagating through the dielectric interface.
On the other hand, if ϵ_r is less than -1, or if it is imaginary, the solution describes a wave that is bound to the surface. These TM surface waves can occur on metals, or other materials with non-positive dielectric constants.

The solution for TE surface waves can be obtained from the foregoing analysis by the principle of duality[7] . If the electric and magnetic fields are exchanged, and μ is substituted for ϵ, the solution above can be applied to the TE case.

4.1.1 Metal Surface

The complex relative dielectric constant of a metal can be expressed in the following form:

$$\epsilon_{rc} = 1 - \frac{j\sigma}{\omega\epsilon_0} \tag{4.17}$$

---

[7] Balanis, *Antenna theory*.

where σ is the conductivity.
For frequencies in the microwave range, the conductivity can be considered real, and much greater than unity, so the dielectric constant is a large and imaginary number. Inserting this equation into (4.14) leads to a simple dispersion relation for surface waves at radio frequencies:

$$k \approx \frac{\omega}{c} \tag{4.18}$$

Thus, surface waves propagate at nearly the speed of light in vacuum, and they travel for many wavelengths along the metal surface with little attenuation. By inserting equation (4.17) into (4.15), we can find an expression for α, the decay constant of the fields into the surrounding medium:

$$\begin{aligned} \alpha &= \frac{\omega}{c}\sqrt{\frac{-1}{2-\frac{j\sigma}{\omega\epsilon_0}}} \\ \alpha &\approx \frac{\omega}{c}\sqrt{\frac{\omega\epsilon_0}{2\sigma}}(1-j) \end{aligned} \tag{4.19}$$

For good conductors at microwave frequencies, the surface waves extend a great distance into the surrounding space. We can also determine γ, the surface wave penetration depth into the metal. By inserting equation (4.17) into equation (4.16), we obtain:

$$\begin{aligned} \gamma = \frac{\omega}{c}\sqrt{\frac{-\epsilon^2}{1+\epsilon}} &\approx \frac{\omega}{c}\sqrt{-\epsilon} = \frac{\omega}{c}\sqrt{\frac{j\sigma}{\omega\epsilon_0}} \\ \gamma \approx (1+j)\sqrt{\frac{\omega\mu_0\sigma}{2}} &= \frac{(1+j)}{\delta} \end{aligned} \tag{4.20}$$

dove δ is the *skin depth* defined like:

$$\delta = \sqrt{\frac{2}{\omega\mu_0\sigma}} \tag{4.21}$$

Thus, the surface currents penetrate only a very small distance into the metal, for example, at 10 GHz the skin depth of copper is less than one micron.

From equation (4.20), it is possible to write an equation for the current in terms of the skin depth, in which E_0 is the electric field at the surface:

$$J_z(x) = \sigma E_z(x) = \sigma E_0 e^{-x(1+j)/\delta} \tag{4.22}$$

The magnetic field at the surface is found by integrating around a path surrounding the thin surface layer of current, extending far into the metal beyond the skin depth:

$$H_0 = \int_0^\infty J_z(x)\,dx = \frac{\sigma\delta}{(1+j)} E_0 \tag{4.23}$$

Thus, the surface impedance of a flat metal surface is

$$Z_s = \frac{E_z}{H_y} = \frac{1+j}{\sigma\delta} \tag{4.24}$$

The surface impedance has equal positive real and positive imaginary parts, so the resistance of a metal surface is driven by an equal amount of inductance.

Consider now an electromagnetic field above a surface of width w and length l used for computing surface impedance; the current in the surface is equal to the magnetic field integrated around the surface

$$I = H_y w \tag{4.25}$$

while the voltage across lenght l is given by the electric field at the surface

$$V = E_z l \tag{4.26}$$

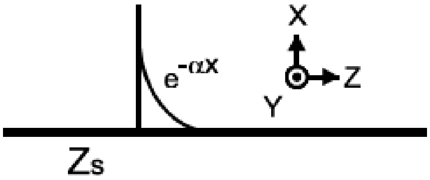

Figure 4.2: A surface wave on an arbitrary impedance surface

The surface impedance can be defined as the ratio of the electric field over the magnetic field at the surface:

$$Z_s = \frac{E_z}{H_y} = \frac{V}{I}\frac{w}{l} \tag{4.27}$$

where the factor of $\frac{w}{l}$ is taken as unity, and the surface impedance defined this way is the same as that given by Ohm's law, expressed in Ohms.

Assume a surface in the YZ plane with general impedance Z_s for which you want to derive the surface wave behavior, like in figure 4.2, and assume that the fields decrease in the x direction with decay constant α, and travel along the z direction with propagation constant k.

For TM surface waves $H_x = H_z = E_y = 0$.

$$E_z = Ce^{-jkz-\alpha x} \tag{4.28}$$

and H_y, from the Ampere's law, is

$$\vec{\nabla} \times \vec{H} = \epsilon\frac{\partial \vec{E}}{\partial t} \tag{4.29}$$

Writing out the derivatives explicitly, and taking into account the three field components that are known to be zero, we obtain the following expression:

$$j\omega\epsilon E_z \;=\; \frac{\partial H_y}{\partial x} \tag{4.30}$$

sostituting in this equation the (4.33), we get

$$H_y \;=\; \frac{-j\omega\epsilon}{\alpha} C e^{-jkz-\alpha x} \tag{4.31}$$

from which it derives the surface impedance for TM surface waves

$$Z_s(TM) \;=\; \frac{j\alpha}{\omega\epsilon} \tag{4.32}$$

TM waves only occur on a surface with positive reactance, or rather an inductive surface impedance.

It is possible also determine the impedance required for TE surface waves, we assume that the electric field is entirely transverse, oriented along the y direction.

Similarly to the TM waves, the magnetic field is

$$H_z \;=\; C e^{-jkz-\alpha x} \tag{4.33}$$

and by Faraday's law

$$\vec{\nabla} \times \vec{E} \;=\; -\mu \frac{\partial \vec{H}}{\partial t} \tag{4.34}$$

from which

$$\frac{\partial E_y}{\partial x} \;=\; -j\omega\mu H_z \tag{4.35}$$

Substituting the (4.33) in the latter, we obtain

$$E_y \;=\; \frac{j\omega\mu}{\alpha} C e^{-jkz-\alpha x} \tag{4.36}$$

The impedance of a surface is taken to be the ratio of the electric and magnetic fields, with an orientation that is consistent with a wave impinging on the surface from outside. This convention ensures that an absorbing surface will have positive resistance, while a surface with reflective gain will have negative resistance. Thus, the surface impedance seen by TE waves is given by the following expression

$$Z_s = -\frac{E_y}{H_z} \tag{4.37}$$

Following this convention, the surface impedance for TE waves is

$$Z_s(TE) = \frac{-j\omega\mu}{\alpha} \tag{4.38}$$

Thus, a negative reactance, a capacitive surface impedance, is necessary to support TE surface waves.

4.2 Comparison of the PEC, PMC, and AMC ground planes

In this section we consider a dipole in close proximity of a PEC, a PMC and an AMC plane. The study is carried out adopting a FEM model.

Planar screens or grid with periodic geometry can be replaced by an anisotropic impedance boundary. The boundary applies a homogeneous characteristic impedance to the surface in an effort to create an equivalent electrical representation of the geometric grid pattern.

So we approximate the AMC surface by a sheet on which the real part of impedance is fixed equal to 10 kΩ.[8]

---

[8] The impedance surface of 10 kΩ is based on simulated values obtain by HIS characterization.

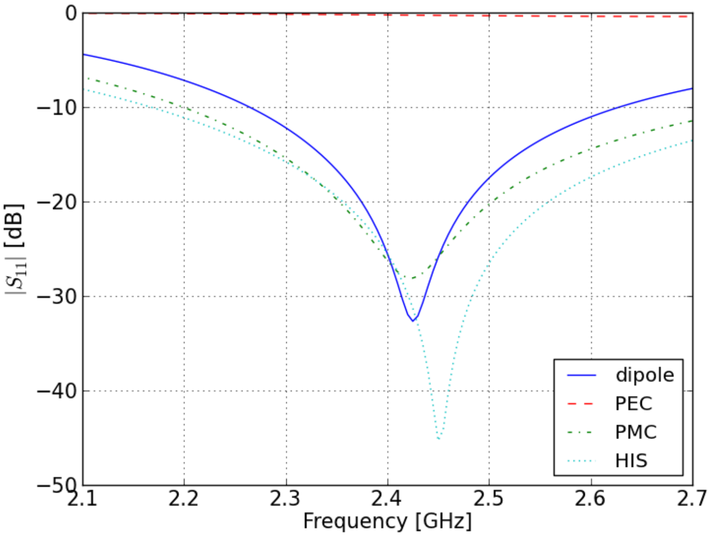

Figure 4.3: Return Loss of a dipole in free-space and placed over PEC, PMC and AMC plane. The dipole is matched to appropriate transmission line impedance.

A dipole length of 57 mm with radius of 0.5 mm and a finite ground plane with 161×161 mm^2 are used to perform this analysis. The dipole height on ground plane is set to 3 mm. The input impedance is matched to a 75 Ω transmission line.

In order to compare the $|S_{11}|$ of a dipole antenna in open space, over a PEC, over a PMC, and finally over an AMC ground plane, see Figure 4.3, the input reference impedance has been appropriately chosen. When the dipole is positioned very close a PMC or an artificial surface, the return loss is around 10 dB because a strong mutual coupling occurs between the image current and the dipole due to their close proximity, and the

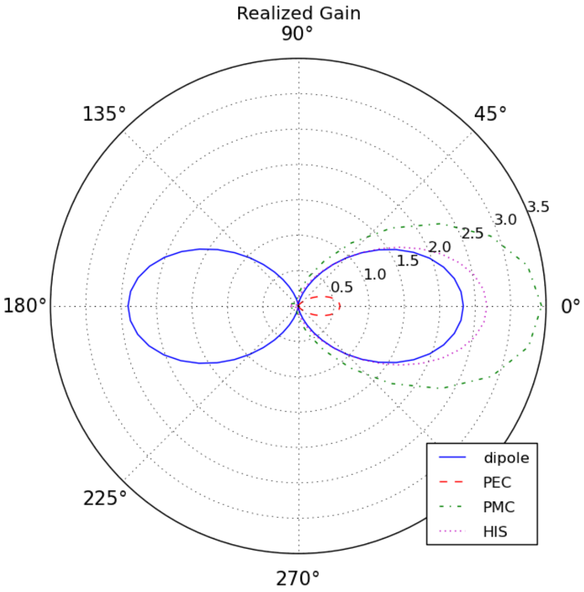

Figure 4.4: Realized Gain of a dipole placed over PEC, PMC and AMC ground plane

input impedance of the dipole is changed. Therefore, the antenna cannot directly match well to a 75 Ω transmission line. It is realized that one can use a proper impedance transformer to obtain a good return loss of the dipole.

When the dipole is placed over a PEC ground plane, the return loss is almost 0 dB because the PEC surface has a 180° reflection phase, so that the direction of the image current is opposite to that of the original dipole. The reverse image current prevents the efficiency of the radiation of the dipole, resulting in a very poor return loss.

When the dipole is positioned near a PMC surface, which has a reflection phase of 0°, the return loss is about 10 dB due to a strong mutual coupling between the image current and the antenna. To obtain a good impedance matching the input-port of the dipole is matched to a 160 Ω transmission line. Moreover, the PMC surface is an ideal surface that does not exist in nature.

A return loss of about -45 dB is achieved by the dipole antenna over the AMC ground plane considering an input-impedance matching of 170 Ω . Because the reflection phase of the AMC surface varies with frequency from 180° to -180° for certain frequency band, the dipole antenna can radiate efficiently.

The radiation patterns are also simulated and shown in figure 4.4.

From this comparison it can be seen that the AMC surface is a good artificial screen for low profile wire antenna.

4.3 Impedance Surface of a Metal Patch

In this section will be calculated the surface impedance of a HISs consisting in an array of simple patch.

The method that we will explain relies on the derivation of an equivalent circuit model for a dense array of metal patch because the field distribution in this periodic structures is very similar to the fields of a single patch antenna[9] . The equivalent model in combination with the functioning of a square patch antenna allows to explain the operation principles of the AMC.

We consider a patch array, with the patch edges length W=L, on

---

[9] Zhang et al., “Planar artificial magnetic conductors and patch antennas”.

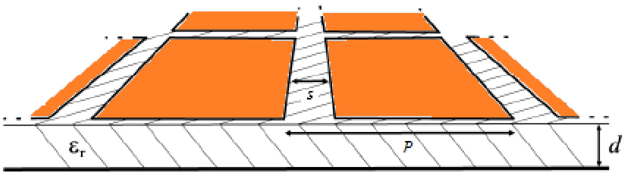

Figure 4.5: Periodic structure of patch array

a homogeneous epoxy substrate with permittivity ϵ_r and thickness d, backed by a ground plane. Also we denote by s the gap length and by P the period of the resulting structure, as shown in figure 4.5.

The major contribution to the overall capacity in this resonant structure comes from the gap discontinuity at both ends of the patch. We denote by C_s the capacity between the patch and the ground plane, by G_s the conductance accounting for radiation, by C_g the interpatch capacity at the main gaps of two patches and by G_s an additional conductance for losses and radiation, as is shown in figure 4.6

For easy treatment the π-network for the gaps are changed to a T-network, this is possible because the electric field is normal to a surface perpendicular to the ground plane in the middle of the gap. The admittances C_g and G_g are divided into two series elements with value $2C_g$ and $2G_g$ which are parallel to the slot impedances C_s and G_s. The final T-network is shown in figure 4.7 within the dotted rectangle. The admittances B and G are given by:

$$B = \omega C_{eq}^{0} = \omega(C_s + 2C_g) \tag{4.39}$$

$$G = (G_s + 2G_g) \tag{4.40}$$

where $C_{eq}^{o} = WC_0$ is a equivalent capacity proportional to the width

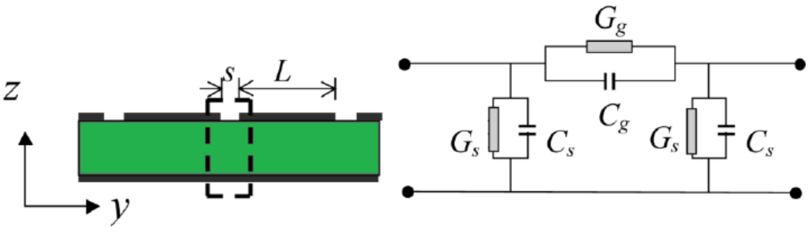

Figure 4.6: Gap discontinuity and its π-network

of the single patch with C_0 the gap capacitance per meter for a given substrate.

The transmission-line model for the patch array is show in figure 4.7 where admittance of one element is[10]

$$Y = G + jB + Y_c \frac{G + j(B + Y_c \tan \beta L}{Y_c - B \tan \beta L + jG \tan \beta L)} \tag{4.41}$$

where β is the propagation constant, L is the patch length and Y_c is the characteristic admittance of the transmission lines. The single unit-cell resonates when the imaginary part of the admittance vanishes, ie when[11]

$$\tan \beta L = \frac{2Y_c B}{G^2 + B^2 - Y_c^2} \tag{4.42}$$

This result present sufficient accuracy only up to frequencies of a few GHz. For a complete characterization of discontinuities a more rigorous full-wave analysis is performed. The transmission line model offers a simple way to create an initial design as a starting point for a numerical optimization.

---

[10] Zhang et al., "Planar artificial magnetic conductors and patch antennas", eq. 4.

[11] Ibid., eq. 5.

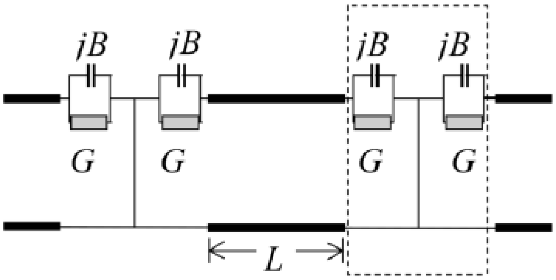

Figure 4.7: Equivalent transmission line network of AMC array patch

4.3.1 FEM AMC Model

To validate the above transmission-line model, it was decided to verify the result shows in[12] by electromagnetic simulator HFSS.

In [12] for a single patch cell resonating at 5.45 GHz, the starting point for an optimization process would be a patch length of 15.95 mm, half the effective wavelength $\lambda_{eff} = 31.89$ mm. The slot capacitance will be $C_s = 9.27$ pF/m, from which it derives a microstrip-gap-discontinuity equivalent capacitance of $C^o_{eq} = 16.03$ pF/m for a gap-length s=0.5 mm. The latter is a factor of 1.73 higher than that of the single patch, so the unit-cell patch length of the array should be shorter by this factor, that is $W = L = 9.22$ mm.

To verify this result, it is not necessary nor possible to simulate an infinite structure, but it suffices to apply mirror boundary conditions around the single unit cell. Also if this has geometrical and electrical symmetry the sidewall can be replaced by appropriate boundary condition.

---

[12] Zhang et al., "Planar artificial magnetic conductors and patch antennas".

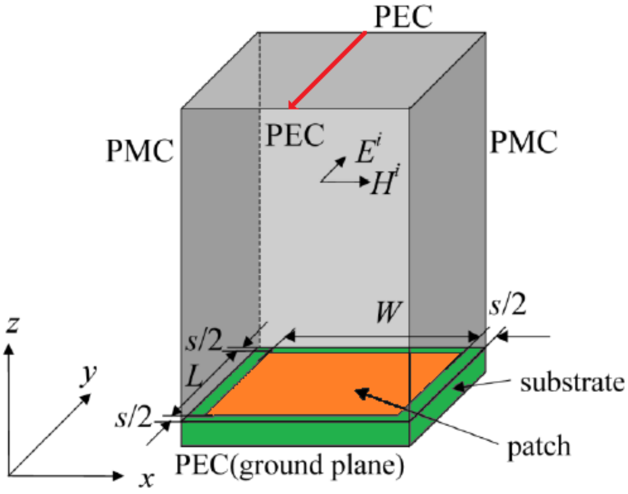

Figure 4.8: AMC Patch Cell

The FEM Model[13] to compute the reflection phase characteristics of the proposed AMC structure is shown in figure 4.8.

This model is based on simulating scattering parameters of a single port air filled waveguide with two perfect electric conductors (PECs) and two perfect magnetic conductors (PMCs) walls. The propagating plane wave is polarized parallel to the PMC walls and normal to the PEC walls. The waveguide is then terminated to a single unit cell and the reflection phase is obtained by calculating the scattering parameter at the input of this single port waveguide.

In our case the unit-cell is a single patch etched on a dielectric substrate with $\epsilon_r = 3.5$ and height $h_{sub} = 1.57$ mm with a patch edges

---

[13] Al-Nuaimi and Whittow, "Novel planar AMC for low profile antenna applications".

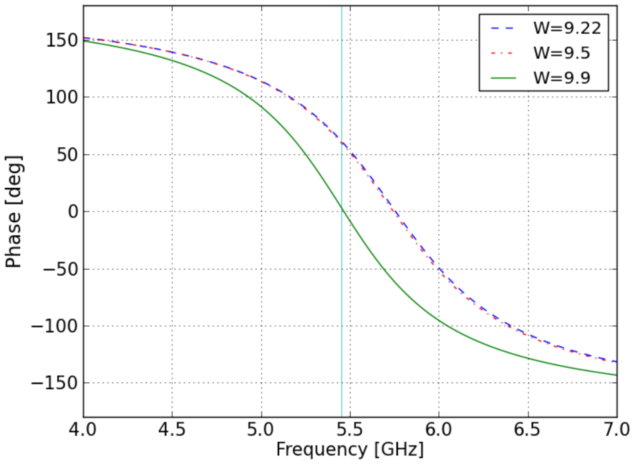

Figure 4.9: Simulated reflection phase of single patch unit-cell

length of $W = L = 9.22$ mm, which is very close to the physical realization length of 9.5 mm.[14]

Figure 4.9 shows the phase of the reflection coefficient returned by FEM simulator for three value of the patch edges length: the physical realization value, $W = 9.5$ mm, the value calculated by the equivalent transmission-line model, $W = 9.22$ mm, and $W = 9.9$ mm is the curve that corresponds to the patch edges length for which the phase is 0° at 5.45 GHz. As can be seen from the figure the results returned by FEM simulator differ slightly from those obtained in[15] with a FTDT simulator. The difference can be ascribed to the different numeric method (and relative mesh property), FEM vs. FTDT, and different excitation

---

[14] Inside unit-cell simulation metals are approximated by PEC boundary.

[15] Zhang et al., “Planar artificial magnetic conductors and patch antennas”.

wave-port vs. plane-wave, used. However, in our approaches we have a greater simplicity and a faster simulations.

The magnitude of the reflection coefficient S_{11}, its phase and the surface impedance of the simulated unit cell are shown on figure 4.10 for patch dimensions of $W = L = 9.9$ mm. The reflection coefficient exhibits 90° around 5.0 GHz and presents an impedance of about 8850 Ω at resonance.

It is clear from this comparison that the patch array surface is a good ground plane candidate for low profile antenna designs.

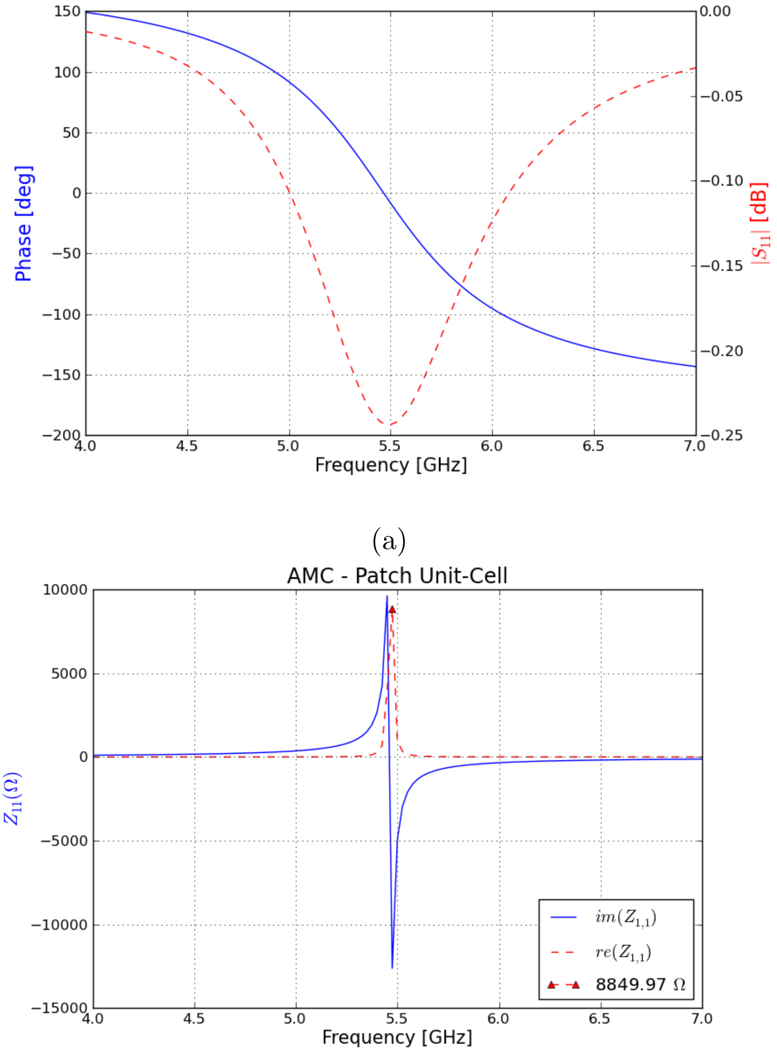

(a)

(b)

Figure 4.10: Simulated result of a single patch unit-cell. (a) Magnitude and phase of the reflection coefficient S_{11}; (b) Surface impedance of the unit cell

4.3.2 Technical Notes

Because the major contribution to the overall capacity in the single patch resonant structure comes from the gap discontinuity at both ends of the patch, to optimize the results obtained by HFSS simulations it was necessary to operate manually on the mesh constructed by the simulator. This technique of guiding HFSS's mesh construction is referred to as *seeding* the mesh. Seeding is performed using the Mesh Operations commands.

We can instruct HFSS to reduce the maximum size of tetrahedral elements on a surface or within a volume until they are below a certain value through the Length-based Mesh Refinement command. The length of a tetrahedron is defined as the length of its longest edge. These types of mesh operations are performed on the current mesh, that is, the most recently generated mesh.

In our case, we have reduced the length of a tetrahedron inside the gap discontinuity at both ends of the patch, halving the default value.

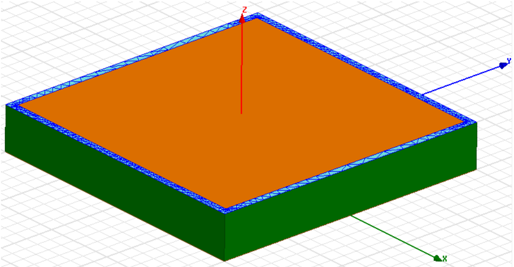

Figure 4.11: Mesh inside the gap discontinuity at both ends of the patch

4.4 Polarization Diversity

In this section we will characterize a square patch unit-cell suitable to obtain a high impedance surface at operating frequency of 5.8 GHz. After this first step, we will modify the layout of square unit-cell to obtain an artificial ground plane that exhibits in-phase reflection coefficients with polarization-dependent feature.

An approach to realize polarization dependence is to design an AMC surface which exhibits a 90° reflection phase for the $\hat{x}$-polarized wave and a $-90°$ reflection phase for the $\hat{y}$-polarized wave. The easiest way to achieve this result is to influence the electrical currents flowing along the $\hat{y}$ direction by modifying the patch length in this direction.[16]

We consider an linearly polarized radiator, such as a 45° oriented dipole over a surface, its total radiated field can be expressed by the summation of directly radiating field, E_d, from the dipole and the reflected field, E_r, from the AMC surface:

$$\begin{aligned}\vec{E} = \vec{E_d} + \vec{E_r} = \frac{E_0}{2}(\hat{x} \cdot e^{-jkz} + \hat{y} \cdot e^{-jkz}) + \\ + \frac{E_0}{2}(\hat{x} \cdot e^{-jkz-2jkd+j\theta_x} + \hat{y} \cdot e^{-jkz-2jkd+j\theta_y})\end{aligned} \tag{4.43}$$

where E_0 is the magnitude of electrical fields, d is the height of the dipole over the ground plane, θ_x is the reflection phase of the ground plane for the $\hat{x}$-polarized incident wave and θ_y for the $\hat{y}$-polarized incident wave. If the dipole is placed very close to the ground plane then $kd \approx 0$.

If the ground plane is a PEC, $\theta_x = \theta_y = 180°$ thus the total radiating field becomes zero because the reflected field cancels the directly radiating

---

[16] Yang and Rahmat-Samii, "Polarization dependent electromagnetic band-gap surfaces: characterization, designs, and applications".

field. If the plane is an AMC,with different reflection proprieties for $\hat{x}$ and $\hat{y}$ direction ($\theta_x = 90°$ while $\theta_y = -90°$) we have:

$$\vec{E} = \frac{E_0}{2} e^{-jkz}[(\hat{x} + \hat{y}) + j(\hat{x} - \hat{y})] \tag{4.44}$$

The reflected field becomes perpendicular to the directly radiating field with a 90° phase difference, and a RHCP electromagnetic wave is obtained.

4.4.1 Polarization-dependent Unit-cell

In order to design an artificial ground plane we take the Zhang's unit-cell characterized in the previous paragraph as layout model.

A FR4-epoxy laminate with $\epsilon_r = 4.6$ and 1.57 mm thickness it was used as substrate of the artificial ground plane,in view of a future inexpensive implementation.
The patch edges length and gap width are designed to achieve a 90° reflection phase at 5.8 GHz. This result was obtained by a square patch unit cell which has edges length equal to 6.95 mm and the gap width between adjacent patches to 0.5 mm. The magnitude of the reflection coefficient S_{11}, its phase and the surface impedance of the simulated unit cell are shown on figure 4.12. The reflection coefficient exhibits an unit-cell impedance about of 5000 Ω/square at resonance.

It is possible to assert that the patch array surface derived by periodic replication of this unit-cell is a good ground plane candidate for low profile antenna designs.

In order to achieved an unit-cell which exhibits a $-90°$ reflection phase for the $\hat{y}$-polarized wave we carry out a parametric study on the patch edge length in $\hat{y}$-direction.

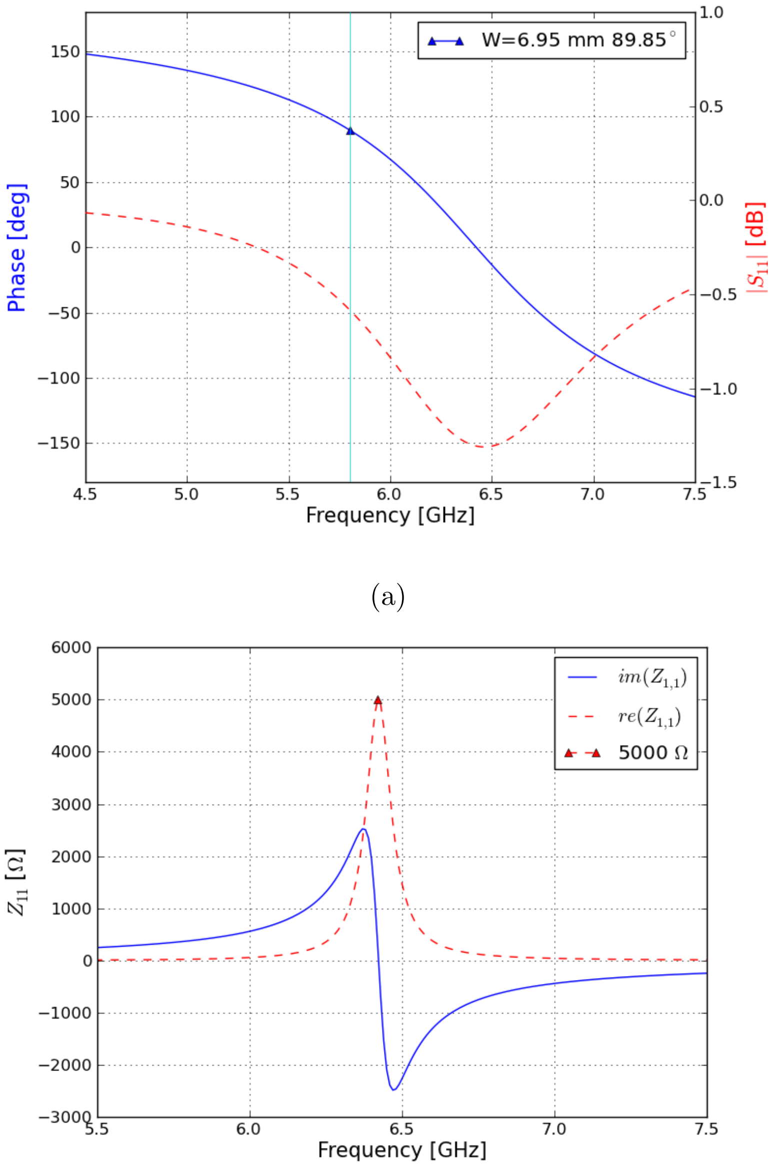

(a)

(b)

Figure 4.12: Simulated reflection coefficient of a square patch unit-cell optimized at 5.8 GHz. (a) Magnitude and phase; (b) Surface impedance.

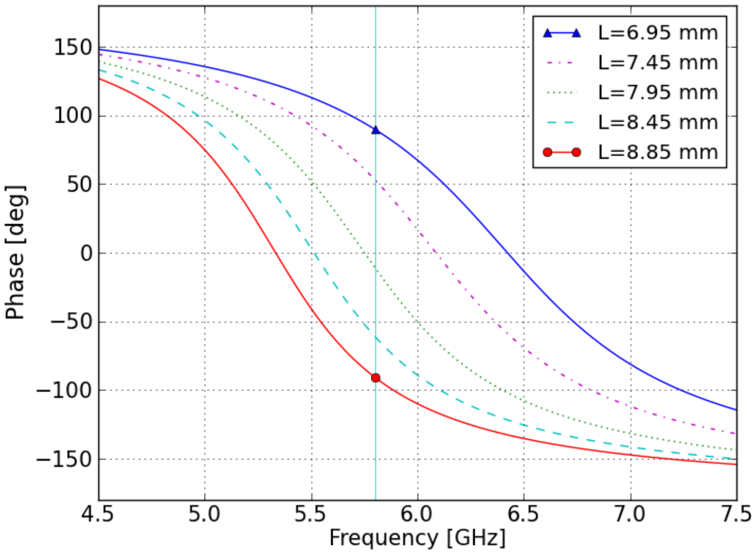

Figure 4.13: Trend of the reflection phase versus patch-lengths

As shown in figure 4.13, the phase of reflection coefficient is -90° at 5.8 GHz by a patch length of 8.85 mm.

In short the polarization-dependent unit-cell is a rectangular patch with the following features:

Parameter	**Dimension**
W	6.95 mm
L	8.85 mm
h_{sub}	1.57 mm
ϵ_r	4.6
$\tan\delta$	0.018

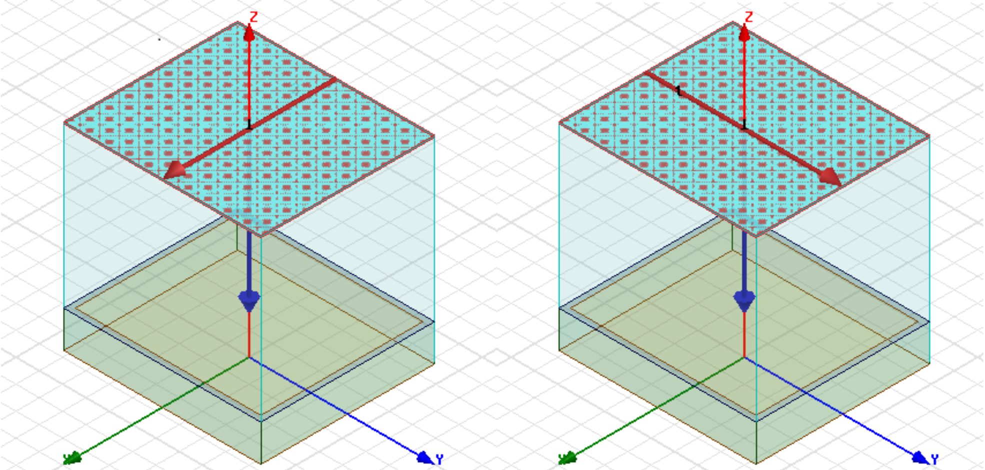

Figure 4.14: FEM Model setup to characterize a rectangular unit-cell.

To compute the feature of the proposed polarization-dependent AMC, a FEM model over the rectangular unit-cell is used. The reflection phase is calculated by computation of the scattering parameter at the waveguide input-port. Two simulation are performed one imposing that the propagating plane wave is polarized along $\hat{x}$-direction and another choosing a $\hat{y}$-polarized wave, as show in figure 4.14. Figure 4.15 shows the surface impedance for both simulations.

To verify the operational mechanism of the AMC surface, a duplication of 5 × 5 rectangular polarization dependent unit-cell is investigated by a 45° oriented planar dipole antenna on this plane, as show in figure 4.16.

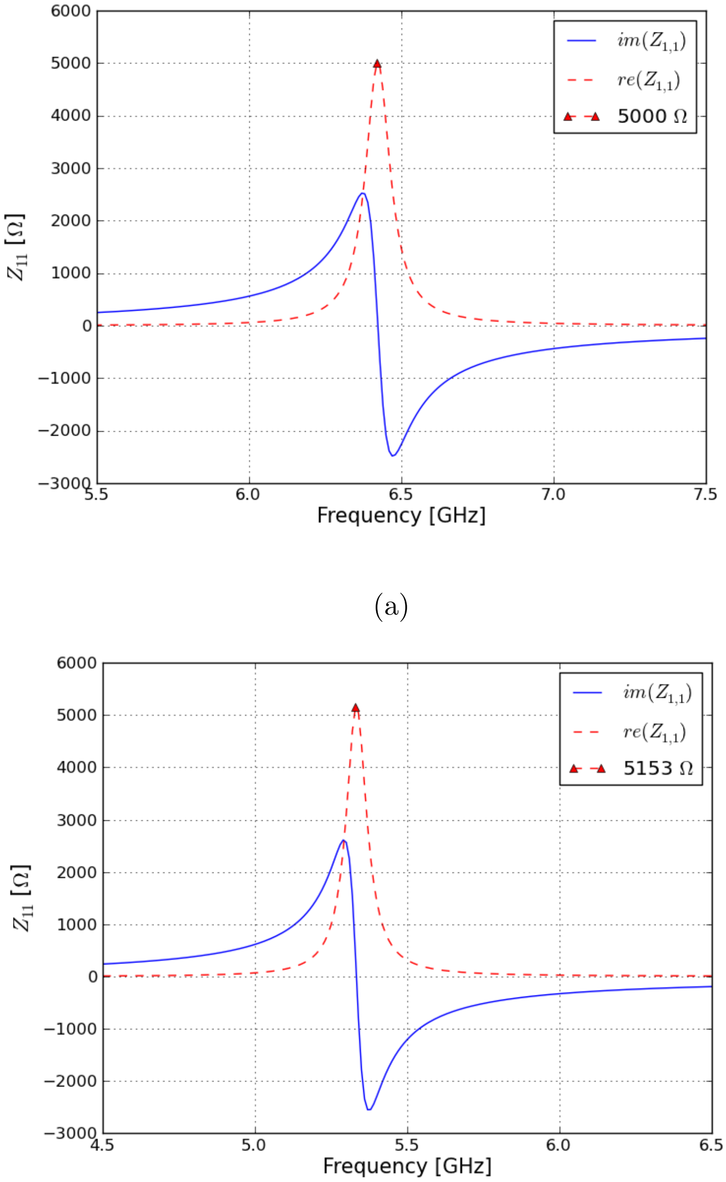

(a)

(b)

Figure 4.15: Simulated impedance surface of rectangular patch unit-cell optimized at 5.8 GHz.

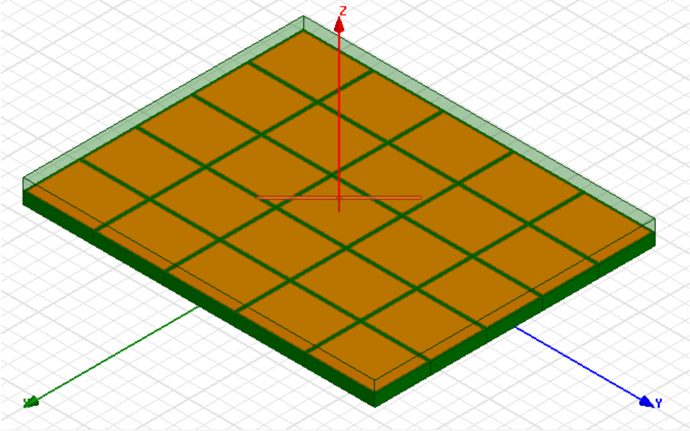

Figure 4.16

From a computational point of view, the faster and less expensive way to test the high impedance surface is to export the dataset of the real and imaginary part of impedance surface in figure 4.15 and modeling the AMC ground plane by a sheet on which to impose an anisotropic impedance boundary (AIB).
Figura 4.17 shows simulated gain pattern at 5.8 GHz, here it is possible to see that a left-hand circular polarization is obtained at boresight.

This result shows that by changing the geometry of a single unit-cell it is possible to obtain circular polarization and in general polarization-diversity. It worth to stress that this was obtained by a model, in which we set an anisotropy condition only along the two main cartesian directions. In reality several variables come into play and only a full-wave simulation allows to obtain a result as close as possible to the real one. Also the AIB-model allows to the electromagnetic radiation to propagate across the artificial plane, so a right polarized back-lobe is present.

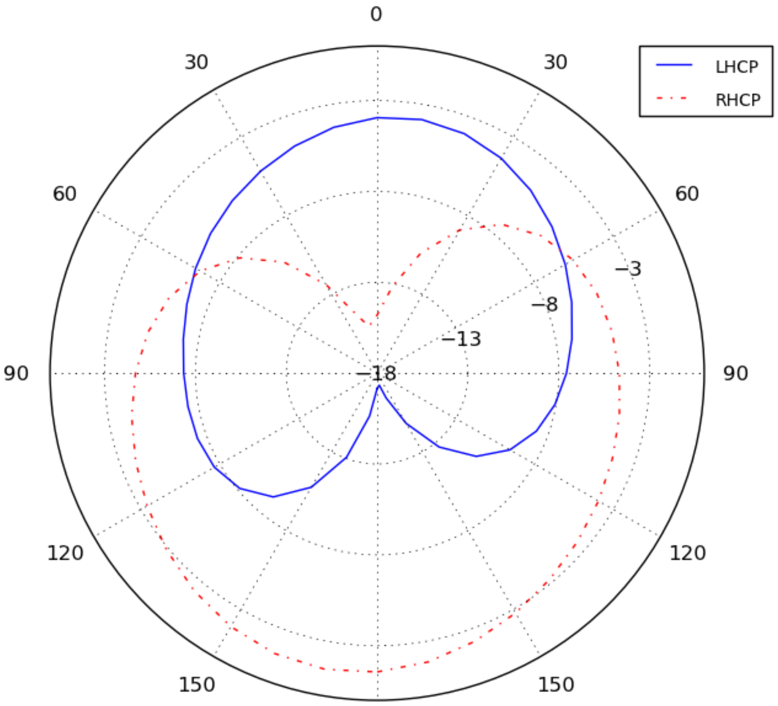

Figure 4.17: Simulated Realized Gain Pattern of the planar dipole over HISs by anisotropic impedance boundary condition.

A drawback of a full-wave simulation is the great requirements of computational resources and the long simulation-time required. This is addressed in HFSS with the introduction of an advanced solving technique called the Domain Decomposition Method (DDM) which enables the use of distributed memory across many different machines to solve very large problems.

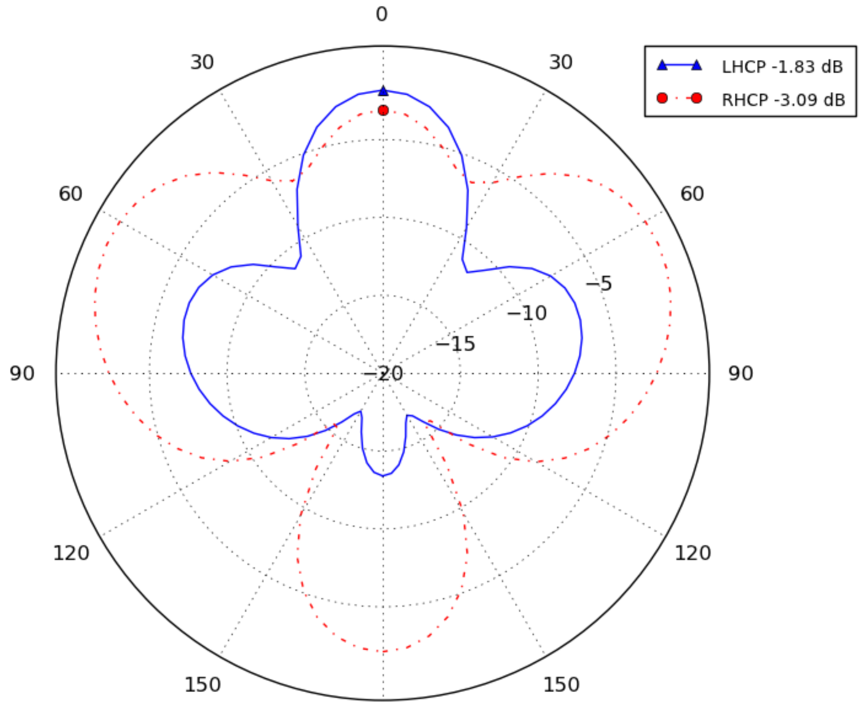

Figure 4.18: Realized Gain Pattern of the planar dipole over HISs by full-wave simulation

By breaking the problem into five computational domains the full-wave simulation was completed in about 30 minutes by a RAM employment of 2.8 GB overall.

Figure 4.18 shows realized gain pattern at 5.8 GHz. It is possible to see that by full-wave simulation we do not get circular polarization, we have an XPD of only 1.26 dB. This is confirmed also by figure 4.19 in which the radiation fields are plotted along the main polar axes ϕ and θ.

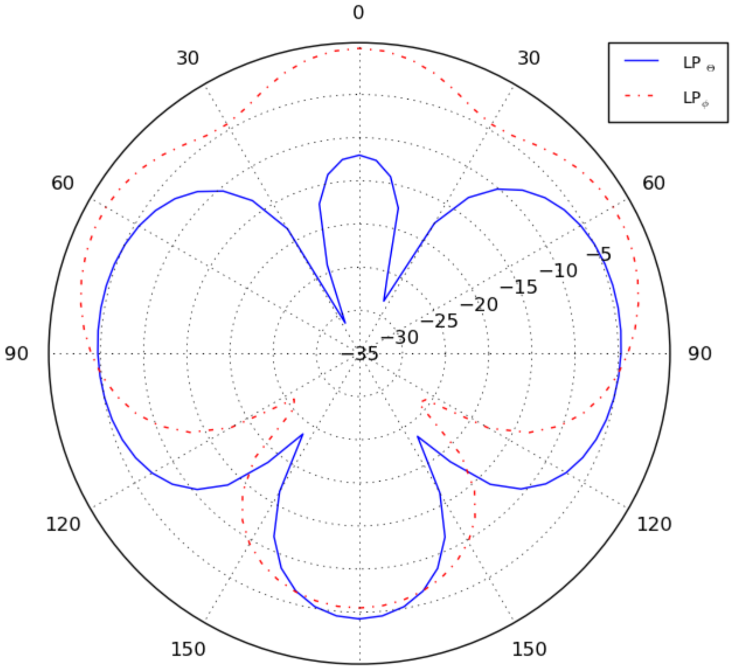

Figure 4.19: Full-wave Realized Gain pattern plotted along ϕ- and θ- polar axes. The ϕ-component radiation prevails resulting in a linear polarization.

To explain why we do not get circular polarization we can investigate the amplitudes and phases of the reflection coefficient, shown in figure 4.20. As you can see there is a delta of amplitude of 1.45 dB at a frequency of 5.8 GHz, while they are equal a 5.91 GHz. If we plot the radiation pattern at this frequency we see that the left circular polarization improves at boresight, as show figure 4.21 where an XPD of 6.67 dB is obtained.

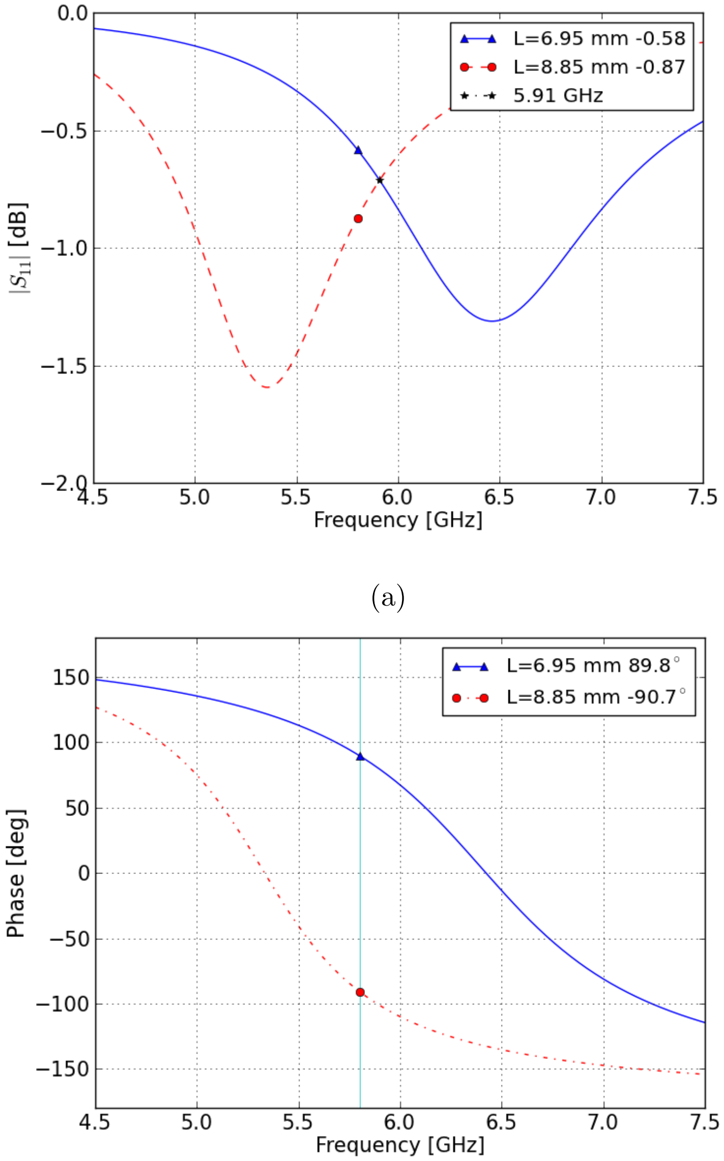

(a)

(b)

Figure 4.20: Simulated reflection coefficient of rectangular patch unit-cell optimized at 5.8 GHz. (a) Magnitudes; (b) Phases.

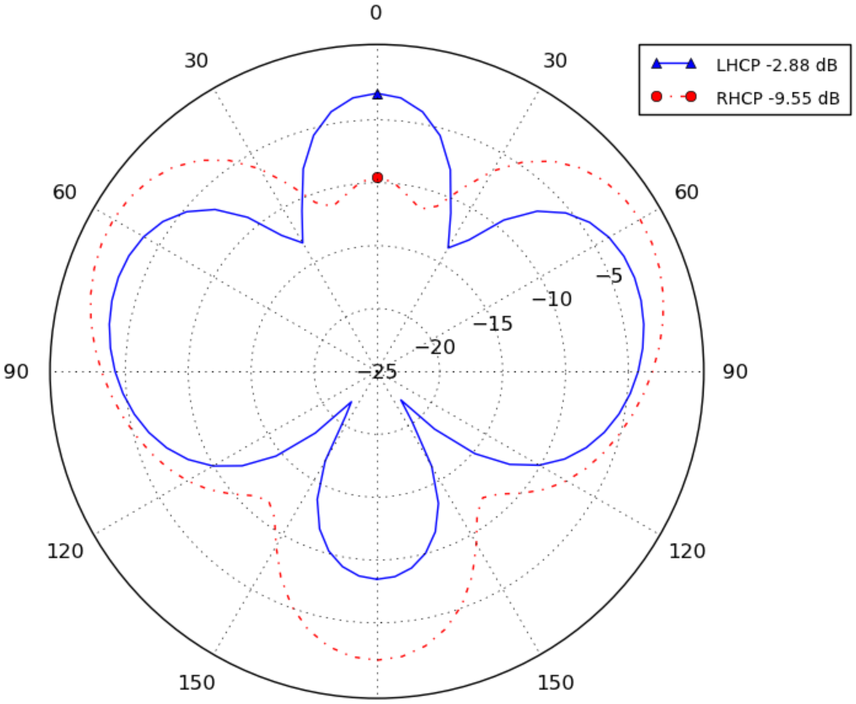

Figure 4.21: Full-wave Realized Gain pattern at 5.9 GHz

To improve the circular polarization we could work appropriately on the two linear components in figure 4.19, these have to be equal in magnitude and in phase quadrature.

The model can also be improved, in first approximation we placed kd = 0 in equation (4.44), while in our case it has a finite value.
If we consider a finite thickness d, the total radiated field becomes

$$\vec{E} = \frac{E_0}{2} e^{-jkz} [(\hat{x} + \hat{y}) + j(\hat{x} - \hat{y}) e^{-jkd}] \tag{4.45}$$

where d=1.57 mm and k= $\frac{2\pi}{\lambda_0}\sqrt{\epsilon_r}$.

On the reflection field is introduced an additional phase shift of about 11° which can be compensated opportunely tuning the HIS.

Conclusions

The goal of this work was the study, the design and the experimental characterization of antennas suitable for short range communications. We propose two planar microstrip patch antennas. A study has been carried out by support of electromagnetic FEM simulators, used for parametric study, in order to achieve circular polarization with Axial Ratio lower than 3 dB at the operating frequency of a Dedicated Short-Range Communication system.

The first prototype proposed and analyzed was a double-layer patch antenna in which the coupling between the feed and the radiating patch is realized through a cross-shaped aperture in the ground plane placed between two layers laminate of Arlon AD450 with the same electromagnetic properties. Appropriately dimensioning the slot sizes and patch lengths left circular polarization is obtained with AR of about 1.7 dB, which corresponds to an XPD of about 20 dB. A LHCP gain of about 5.52 dBc was estimated by Gain Comparison Method.

The second prototype proposed was realized by CNC milling machine and it was a patch circular disc slotted by a concentric elliptical cut with coaxial feed design su FR4 epoxy. Appropriately dimensioning the slot sizes left circular polarization is obtained with AR of about 1.3 dB, which corresponds to an XPD of about 22.5 dB. A LHCP gain of about 4.68 dBc was estimated by a non-canonical method of polarization measurement.

The results returned from the experimental measurements fulfill the DSRC standard requirements and are obtained with very compact designs. This is required for a small antenna suitable for a On Board Unit of an Electronic Toll Collection system.

The last section was dedicated to the High-Impedance Surfaces, an innovative microwave device used to improve performance of low profile antennas. Through full-wave FEM-simulations these HIS were characterized by studying the single unit-cell on which we impose appropriate periodic boundary conditions. Moreover, a simple polarization-dependence HIS has been optimized at 5.8 GHz, by anisotropic impedance boundary model and by full-wave simulation. This anisotropic HIS can be used to produce circular polarized wave. The results confirm that a simple rectangular patch array can be used as artificial ground plane to reduce the profile of planar antennas and simultaneously achieve polarization diversity.

Bibliography

Aksun, M Irsadi, S-L Chuang, and Yuen Tze Lo. "On slot-coupled microstrip antennas and their applications to CP operation-theory and experiment". In: *Antennas and Propagation, IEEE Transactions on* 38.8 (1990), pp. 1224–1230.

Al-Nuaimi, M.K.T. and W.G. Whittow. "Novel planar AMC for low profile antenna applications". In: *Antennas & Propagation Conference, 2009. LAPC 2009. Loughborough.* IEEE. 2009, pp. 145–148.

Ayad, H. et al. "Performances of low profile dipole antenna AMC-based surface using metamaterials structures". In: *Telecommunications (ICT), 2012 19th International Conference on.* IEEE. 2012, pp. 1–5.

Balanis, C.A. *Antenna theory.* J. Wiley, New York, 1997.

Cutler, CC, AP King, and WE Kock. "Microwave antenna measurements". In: *Proceedings of the IRE* 35.12 (1947), pp. 1462–1471.

European Standard EN 12253, Comité Européen de Normalisation (CEN), Jul., 2004.

Gupta, K. C. and P. C. Sharma. "Segmentation and Desegmentation Techniques for the Analysis of Two Dimensional Microstrip Antennas". In: *IEEE AP-S Int. Symp. Digest* (1981), pp. 19–22.

Hsieh, Gui-Bin, Ming-Huang Chen, and Kin-Lu Wong. "Single-feed dual-band circularly polarised microstrip antenna". In: *Electronics Letters* 34.12 (1998), pp. 1170–1171.

Huang, Chih-Yu, Jian-Yi Wu, and Kin-Lu Wong. "Cross-slot-coupled microstrip antenna and dielectric resonator antenna for circular polarization". In: *Antennas and Propagation, IEEE Transactions on* 47.4 (1999), pp. 605–609.

Huang, John. "A technique for an array to generate circular polarization with linearly polarized elements". In: *Antennas and Propagation, IEEE Transactions on* 34.9 (1986), pp. 1113–1124.

Iwasaki, Hisao. "A circularly polarized small-size microstrip antenna with a cross slot". In: *Antennas and Propagation, IEEE Transactions on* 44.10 (1996), pp. 1399–1401.

Jazi, MN and MN Azarmanesh. "Design and implementation of circularly polarised microstrip antenna array using a new serial feed sequentially rotated technique". In: *IEE Proceedings-Microwaves, Antennas and Propagation* 153.2 (2006), pp. 133–140.

Lo, YT, B Engst, and RQ Lee. "Technical memorandum: Simple design formulas for circularly polarised microstrip antennas". In: *IEE Proceedings H (Microwaves, Antennas and Propagation).* Vol. 135. 3. IET. 1988, pp. 213–215.

Lu, Jui-Han, Chia-Luan Tang, and Kin-Lu Wong. "Circular polarisation design of a single-feed equilateral-triangular microstrip antenna". In: *Electronics Letters* 34.4 (1998), pp. 319–321.

Munson, R. "Conformal microstrip antennas and microstrip phased arrays". In: *Antennas and Propagation, IEEE Transaction on* 22.1 (1974), pp. 74–78.

Newman, E and Pravit Tulyathan. “Analysis of microstrip antennas using moment methods”. In: *Antennas and Propagation, IEEE Transactions on* 29.1 (1981), pp. 47–53.

Orfanidis, S.J. *Electromagnetic Waves and Antennas.* Online book, 2004, pp. 280–284. URL: `www.ece.rutgers.edu/~orfanidi/ewa`.

Pozar, DAVIDM. “A reciprocity method of analysis for printed slot and slot-coupled microstrip antennas”. In: *antennas and propagation, ieee transactions on* 34.12 (1986), pp. 1439–1446.

Richards, W and Y Lo. “Design and theory of circularly polarized microstrip antennas”. In: *Antennas and Propagation Society International Symposium, 1979.* Vol. 17. IEEE. 1979, pp. 117–120.

Richards, W., Y. Lo, and D. Harrison. “An improved theory for microstrip antennas and applications”. In: *Antennas and Propagation, IEEE Transactions on* 29.1 (1981), pp. 38–46.

Sheen, David M et al. “Application of the three-dimensional finite-difference time-domain method to the analysis of planar microstrip circuits”. In: *Microwave Theory and Techniques, IEEE Transactions on* 38.7 (1990), pp. 849–857.

Sievenpiper, D. et al. “High-impedance electromagnetic surfaces with a forbidden frequency band”. In: *Microwave Theory and Techniques, IEEE Transactions on* 47.11 (1999), pp. 2059–2074.

Silvester, P. “Finite element analysis of planar microwave networks”. In: *Microwave Theory and Techniques, IEEE Transactions on* 21.2 (1973), pp. 104–108.

Standard, IEEE. “IEEE Standard Test Procedures for Antennas”. In: *IEEE Standard* (1979).

Sullivan, P and D Schaubert. “Analysis of an aperture coupled microstrip antenna”. In: *antennas and propagation, ieee transactions on* 34.8 (1986), pp. 977–984.

Teshirogi, Tasuku, Masato Tanaka, and Wataru Chujo. “Wideband circularly polarized array antenna with sequential rotations and phase shift of elements”. In: *Antennas and Propagation Society International Symposim* (1985), pp. 117–120.

Toh, Bee Yen, Robert Cahill, and Vincent F Fusco. “Understanding and measuring circular polarization”. In: *Education, IEEE Transactions on* 46.3 (2003), pp. 313–318.

Wong, Kin-Lu and Yi-Fang Lin. “Circularly polarised microstrip antenna with a tuning stub”. In: *Electronics Letters* 34.9 (1998), pp. 831–832.

Yang, F. and Y. Rahmat-Samii. “Reflection phase characterizations of the EBG ground plane for low profile wire antenna applications”. In: *Antennas and Propagation, IEEE Transactions on* 51.10 (2003), pp. 2691–2703.

Yang, Fan and Yahya Rahmat-Samii. “A low profile single dipole antenna radiating circularly polarized waves”. In: *Antennas and Propagation, IEEE Transactions on* 53.9 (2005), pp. 3083–3086.

— “Polarization dependent electromagnetic band-gap surfaces: characterization, designs, and applications”. In: *Antennas and Propagation Society International Symposium, 2003. IEEE.* Vol. 3. IEEE. 2003, pp. 339–342.

Zhang, Y. et al. “Planar artificial magnetic conductors and patch antennas”. In: *Antennas and Propagation, IEEE Transactions on* 51.10 (2003), pp. 2704–2712.